DEUTSCHES ELEKTRONEN-SYNCHROTRON DESY

DESY 74/11
March 1974

Photoproduction of ρ^0, ω and ρ^- Mesons on Deuterons at Energies between 1 and 5 GeV

by

P. Benz, O. Braun, H. Butenschön, D. Gall, U. Idschok, C. Kiesling, G. Knies, K. Müller, B. Nellen, R. Schiffer, P. Schlamp, H. J. Schnackers, P. Söding, J. Stiewe and F. Storim

(Aachen-Bonn-Hamburg-Heidelberg-München Collaboration)

2 HAMBURG 52 · NOTKESTIEG 1

To be sure that your preprints are promptly included in the
HIGH ENERGY PHYSICS INDEX ,
send them to the following address (if possible by air mail) :

DESY
Bibliothek
2 Hamburg 52
Notkestieg 1
Germany

Photoproduction of ρ^0, ω and ρ^- Mesons on Deuterons at Energies between 1 and 5 GeV

by

P. Benz[§], O. Braun[+], H. Butenschön[§], D. Gall[§], U. Idschok[†], C. Kiesling[x], G. Knies[§], K. Müller[†], B. Nellen[†], R. Schiffer[*], P. Schlamp[x], H.J. Schnackers[*], P. Söding[§], J. Stiewe[+] and F. Storim[§]

(Aachen - Bonn - Hamburg - Heidelberg - München Collaboration)

Abstract:

The reactions $\gamma d \to \rho^0 d$, $\gamma d \to \omega d$ and $\gamma n \to \rho^- p$ have been investigated in a deuterium bubble chamber experiment at DESY with a bremsstrahlung beam of 5.5 GeV maximum energy. Effective mass distributions as well as total and differential cross sections are presented. The results are compared with ρ^0 and ω production on protons.

* III. Physikalisches Institut, Lehrstuhl B der technischen Hochschule Aachen

† Physikalisches Institut der Universität Bonn

§ DESY und II. Institut für Experimentalphysik der Universität Hamburg

+ Institut für Hochenergiephysik der Universität Heidelberg

x Max-Planck-Institut für Physik und Astrophysik München

1. Introduction

Photoproduction of neutral vector mesons is known to be a strongly diffractive process. The quantum numbers of the incoming and outgoing particles are identical, as in elastic scattering. Well established properties of diffractive vector meson production are the approximate independence of the amplitude on energy associated with a small real part, the predominant exchange of natural parity, and the nearly complete conservation of the boson's s-channel helicity.

The isospin properties of vector meson photoproduction are less well known. For a study of these properties experiments with neutron or deuteron targets are necessary. In most of the vector meson photoproduction experiments on deuterium carried out so far, the sum of the coherent and break-up cross sections was measured.[1] Since the break-up process is difficult to analyze, interpretation of the results usually involves an extrapolation to $|t|_{min}$ where the incoherent part becomes small. Indications were obtained for a non-negligible I = 1 exchange contribution to ρ^o photoproduction on nucleons at $t \approx 0$ for photon energies of about 5 GeV.[1]

An experimentally cleaner way to investigate the isospin properties is to measure the coherent production

$$\gamma d \to \rho^o d \qquad (1)$$

separately, by detecting the final state deuteron. This was done in a counter experiment at SLAC where coherent ρ^o production was measured in the double scattering region at large $|t|$; hence the contribution from elastic $\rho^o N$ scattering could be investigated.[2] At smaller $|t|$ in the single scattering diffractive region reaction (1) has been measured by this group at DESY[3] and by a Weizmann group[4]; these were low statistics bubble chamber experiments. In the present paper, we present results with improved statistics in the energy region $0.9 < E_\gamma < 5.3$ GeV for $|t| < 0.2$ GeV^2. In the same experiment we have also observed coherent ω photoproduction

$$\gamma d \to \omega d. \qquad (2)$$

In ρ photoproduction, I = 1 exchange can also be studied in pure form in the charge exchange reaction

$$\gamma n \to \rho^- p. \qquad (3)$$

Unfortunately, it is a difficult reaction to measure. We have published some cross sections previously[5] which were obtained from half of the statistics, and are now presenting our final results.

In section 2 of this paper we describe the event identification and the experimental corrections. The effective mass distributions and cross sections for the reactions (1), (2) and (3) are presented in section 3. The discussion of the results follows in section 4 with a determination of the coupling constant ratio $g^2_{\gamma\omega}/g^2_{\gamma\rho}$, an analysis of the isospin structure of the ρ^o and ω photoproduction amplitude on nucleons and a test of Harari-Freund duality and Regge factorization.

2. Experimental Procedure and Identification of final States

The experiment was performed in the 85 cm deuterium bubble chamber at DESY, exposed to a bremsstrahlung beam of 5.5 GeV maximum energy. About 3.1 million pictures were taken. Details about the beam, the determination of the photon spectrum, and the scanning and measuring of the pictures have been described elsewhere.[3,6,7] A total of 85 000 photoproduction events were analyzed. For the kinematic analysis the program CRIND was used[8]. A description of the fitting procedure and a list of the reaction hypotheses considered were given in a previous publication.[7]

2.1 The Reaction $\gamma d \to \pi^+\pi^- d$

To identify the events belonging to the reaction

$$\gamma d \to \pi^+\pi^- d \qquad (4)$$

the following criteria were applied:

(i) There had to be a three constraint (3c) kinematic fit to reaction (4) with a χ^2 probability $P(\chi^2) > 0.1$ %.

(ii) The agreement between the calculated and observed ionization of all tracks had to be satisfactory, and range-energy constraints had to be fulfilled.

(iii) The momentum $|\vec{p}_d|$ of the final state deuteron in the laboratory system had to be $|\vec{p}_d| < 0.45$ GeV/c, corresponding to $t = (p_\gamma - p_{\pi^+\pi^-})^2 > -0.2$ GeV^2. This was required because on part of the pictures only events with $|\vec{p}_d| \leq 0.56$ GeV/c had been measured.

We found 3551 events satisfying these criteria. Among these events, 45 % had only two prongs, since the deuteron track was invisible; the deuteron laboratory momentum is then $|\vec{p}_d| \lesssim 0.165$ GeV/c. Studies with Monte-Carlo simulated events showed that a reliable distinction between reaction (4) and the deuteron break-up reaction

$$\gamma d \to \pi^+ \pi^- pn \qquad (5)$$

is not possible for 2-prong events[3]. Therefore we had to restrict ourselves to the three-prong events (which have a visible deuteron track). For further analysis we only used the three-prong events in the t range $0.04 < |t| < 0.20$ GeV^2, since the fraction of two-prong events in this kinematic range is small and can be corrected for (see below). We found 1061 of these events in the photon energy range $0.9 < E_\gamma < 5.3$ GeV.

As a check for possible biases in the kinematic fits we have investigated the pulls[7]. As is seen in fig.1, they are symmetrically distributed around zero.

To check the event identification we generated Monte Carlo events of reaction (4) and of other reactions, and subjected them to our selection procedure as described above. For the Monte Carlo events the identification of reaction (4) was found to be free from bias within better than 1 %. For true events, however, the situation may be worse due to various effects unknown in detail, which may not have been properly simulated in the Monte Carlo calculations. Thus, for example, true events from reaction (4) may fail the 3c-fit due to an unnoticed scatter of the deuteron near the event vertex. Most of the events which fail the 3c-fit will fall into the sample assigned to reaction (5) for which only a 0c-fit is required. (For some of these events the reaction hypothesis $\gamma d \to \pi^o \pi^+ \pi^- d$ is also possible, but nearly all (>98 %) of the events that fit the latter reaction also fit reaction (5).) In the spurious 0c-fits to reaction (5), the angle between the momenta of the reconstructed neutron and the proton is always small, corresponding to a small proton-neutron effective mass. Furthermore, these fits will always have a spurious proton momentum $|\vec{p}_p|$ greater than the calculated neutron momentum $|\vec{p}_n|$, since momentum balance requires $\vec{p}_p + \vec{p}_n = \vec{p}_d$ whereas for a stopping deuteron $\vec{p}_p \simeq 0.6\, \vec{p}_d$ from the range and for a leaving deuteron $\vec{p}_p \approx \vec{p}_d$ from curvature. Indeed there is an indication of an excess at 0^o in the distribution of the laboratory break-up angle between the proton and the neutron, for the events that fit reaction (5)

but not reaction (4) and that have $|\vec{p}_p| > |\vec{p}_n|$; no such irregularity is observed for events with $|\vec{p}_p| < |\vec{p}_n|$ (see fig.2). From this excess the fraction of the events of reaction (4) that fail the kinematic fit and turn up in the event sample of reaction (5) could be estimated. It leads to a correction that depends on t and reaches +10 % at large $|t|$.

There are also events of reaction (4) that fail the kinematic fits to both reactions (4) and (5). In that case they cannot be fitted by any hypothesis at all. These losses add to the losses of events which were unmeasurable for various reasons and necessitate an overall correction of (+5 ± 2)%. The correction for losses of events at the scanning stage is (+5 ± 3)%.

Finally, since we use only three-prong events in the analysis a further correction has to be made for three-prong events being mistaken as two-prong events. This can occur when the deuteron track is overlapping in the film plane with one of the outgoing pion tracks. Azimuthal symmetry of the tracks around the beam direction was used[9] to correct for this effect, which particularly affects the events at small $|t|$ (up to about +10 %).

In summary we have obtained 1061 three-prong events of reaction (4) in the kinematic region $0.9 < E_\gamma < 5.3$ GeV and $0.04 < |t| < 0.20$ GeV^2. This sample is free of contamination but has to be corrected for various types of inefficiencies. The correction depends on t (+20 % on the average). All cross sections presented below are given a systematic error of ±7 % which includes the uncertainties of the experimental corrections as well as those of the shape and normalization of the photon energy spectrum.

2.2 The Reaction $\gamma d \to \omega d$

To investigate coherent ω production on the deuteron we have to study the reaction

$$\gamma d \to \pi^o \pi^+ \pi^- d. \qquad (6)$$

Since this reaction allows only a kinematic 0c-fit, it cannot be separated from other 0c fit reactions like, e.g., reaction (5). Fortunately the ω is a rather narrow resonance which stands out clearly above the background. Therefore, we can separate the ω from the background directly in the effective $\pi^o\pi^+\pi^-$ mass distributions of all events which are compatible with reaction (6)

according to kinematics and ionization of the tracks. There were 865 such events with three visible tracks in the kinematic range $1.4 < E_\gamma < 5.3$ GeV and $0.05 < |t| < 0.20$ GeV^2. The corrections for scanning losses of three-prong events and for losses of unmeasurable events are the same as for reaction (4).

2.3 The Reaction $\gamma d \to \pi^o \pi^- pp$

Finally we discuss the selection of events belonging to the reaction

$$\gamma d \to \pi^o \pi^- pp. \qquad (7)$$

A kinematic discrimination between reaction (7) and the reaction $\gamma d \to \pi^- pp$ is possible and has been discussed in detail in a previous paper[7]. However, kinematic ambiguities of the 0c-fit to reaction (7) exist with the reactions $\gamma d \to \pi^+ \pi^- d$, $\gamma d \to \pi^o \pi^+ \pi^- d$, $\gamma d \to \pi^+ \pi^- pn$ and $\gamma d \to \pi^o \pi^- pp + m\pi^o (m \geq 1)$. The ambiguity with the first three reactions is due to insufficient $\pi^+/p/d$ discrimination at high laboratory momenta; it can be avoided by a restriction to small $-t = -(p_\gamma - p_{\pi^o\pi^-})^2$. For the study of ρ^- production we therefore used only events in the kinematic region $|t| < 1.1$ GeV^2.

On the other hand, a separation of the single π^o reaction (7) from multiple π^o events is not possible by kinematics or ionization. (Note that the photon energy was not measured, but had to be calculated from energy and momentum conservation.) Therefore we always have to take this background into account when we try to extract ρ^- cross sections. This will be further discussed in section 3.3.

The corrections applied to the data include corrections for scanning losses (+5 %), events with no acceptable hypotheses (+4 %), and events that give spurious fits to the reaction $\gamma d \to \pi^- pp$ (+4 %). Furthermore, the effect of the finite photon energy resolution was unfolded from the photon energy dependence of the cross sections. These finite resolution effects are due to measuring errors and to systematic shifts of the calculated kinematical quantities in case of two-prong events, where the momentum of the invisible proton was fixed at zero in the kinematic fit. The systematic uncertainties of these corrections as well as those of the shape and normalization of the photon energy spectrum sum up to ±12 %, which are included in the error bars of all cross sections given below.

The extraction of information from reaction (7) on the reaction

$$\gamma n \to \pi^o \pi^- p \qquad (8)$$

by means of the spectatormodel will be discussed in section 3.31.

3. Experimental Results

3.1 The Reaction $\gamma d \to \rho^o d$

3.11 Cross Section for the Reaction $\gamma d \to \pi^+ \pi^- d$

The cross section of the reaction (4), $\gamma d \to \pi^+ \pi^- d$, is shown in fig.4a as a function of the laboratory photon energy E_γ between 0.9 and 5.3 GeV. For the reasons discussed in section 2.1, the t range is restricted to $0.04 < |t| < 0.20$ GeV^2 where $t = (p_\gamma - p_{\pi^+\pi^-})^2$.

3.12 ρ^o Production

The effective mass distributions of the $\pi^+\pi^-$, $\pi^+ d$ and $\pi^- d$ systems in reaction (4) are shown in figs. 3a-c for various intervals of E_γ. The production of the ρ^o is the only apparent resonance production process. In fact there is very little background underneath the ρ^o resonance for $E_\gamma > 1.8$ GeV. For $E_\gamma < 1.4$ GeV, on the other hand it is not easy to determine how much ρ^o is present due to the kinematic limitations on t and $M_{\pi^+\pi^-}$. (Note that the minimum photon energy required to produce a ρ^o of resonance mass at $|t| = 0.04$ GeV^2 on deuterons is $E_\gamma = 1.64$ GeV.) Hence the amount of ρ^o deduced is strongly dependent on the mass shapes assumed for the resonance and the background. The $\pi^+ d$ and $\pi^- d$ mass distributions are well described by ρ^o reflection plus phase space background, as we will show below.

The cross section for coherent ρ^o production (reaction (1)) has been determined by fits to the data shown in fig.3. Three different assumptions on the resonance shape were used:

(i) In the first fit, we used a ρ^o Breit-Wigner enhancement which was multiplied by a factor $(M_\rho/M_{\pi\pi})^{n(t)}$ and was added incoherently to a phase space background term[10]. Both resonance and background terms were multiplied by a factor exp(24 t) to describe the experimental t distribution (see below). Besides the amounts of resonance and background, also the

parameters M_ρ, Γ_ρ and n were fitted. From all the fits to the data for $E_\gamma > 1.4$ GeV we found $M_\rho = (0.762 \pm 0.005)$ GeV, $\Gamma_\rho = (0.152 \pm 0.005)$ GeV and $n(t) = (5.6 \pm 0.5) + (14.9 \pm 5.8)\ \text{GeV}^{-2} \cdot t$. The curves shown in fig.3 are obtained from these fits.

(ii) Another assumption was to have a diffractive resonance amplitude T_ρ interfering with the Drell one-pion exchange terms T_D[11,12,13]. The $\pi^\pm d$ elastic scattering amplitudes entering in the Drell terms were calculated from the $\pi^\pm p$ elastic scattering amplitudes in the impulse approximation[14]. The complete amplitude is

$$T_\rho + T_D \exp(i\delta) \cos\delta \qquad (9)$$

where δ is the elastic $\pi^+\pi^-$ scattering phase shift. The factor $\exp(i\delta)\cos\delta$ modifies the Drell terms such as to avoid double counting of ρ^o resonance production[15,16,17]. Since the Drell terms can be calculated, only the resonance amplitude T_ρ was fitted.

(iii) The factor $\exp(i\delta)\cos\delta$ causes the non-resonant term in (9) to vary relatively rapidly in the neighbourhood of the ρ^o, in contrast with the behaviour generally associated with a non-resonant background amplitude. One may therefore redefine the resonant part of the amplitude by splitting the complete amplitude (9) into a slowly and a rapidly varying part[18],

$$T_\rho + T_D \exp(i\delta) \cos\delta \equiv T_\rho + T_D\,(1 + i \exp(i\delta) \sin\delta)$$

$$\equiv T_{res} + T_D,$$

with

$$T_{res} = T_\rho + i\, T_D \exp(i\delta) \sin\delta. \qquad (10)$$

We will also give the ρ^o cross sections obtained with this definition of the resonant part.

3.13 Total and differential Cross Sections for the Reaction $\gamma d \to \rho^o d$

The cross sections $\sigma(\gamma d \to \rho^o d)$ determined with each of these three different assumptions are shown in fig. 4b.* The different assumptions lead to nearly identical cross section values, except in the region $E_\gamma < 1.4$ GeV where threshold effects make the analysis somewhat uncertain. After a steep rise

---

* The cross section values of fig.4b supersede the preliminary results from our earlier publication[3]. The final results presented here are obtained from better statistics, improved experimental corrections and a refined analysis of ρ^o production.

above threshold, the cross section is energy-independent as expected for a purely diffractive production mechanism.

Differential ρ^o production cross sections were determined from the data by repeating the above fits independently in various t bins. The results for $E_\gamma > 1.8$ GeV are shown in fig.5. The differential cross section values obtained with assumption (iii) do not differ from those obtained with assumption (ii) and therefore are not shown in fig.5. The results of the Weizmann group[4] for $d\sigma/dt(\gamma d \to \rho^o d)$ at $E_\gamma = 4.3$ GeV are also shown in fig. 5 (diamonds). They seem to be systematically smaller than ours. We cannot explain this discrepancy but are confident that our normalization cannot be grossly wrong (cf. section 2.1 and ref. 7).

For comparison with differential cross sections of other processes like $\gamma d \to \omega d$ or $\gamma p \to \rho^o p$, it is useful to correct for the kinematic turnover of $d\sigma/dt$ at small $|t|$ (see fig.5) which arises from the fact that for fixed E_γ the kinematically possible maximum value of $M_{\pi^+\pi^-}$ depends on t, thus producing a variable cutoff in the mass distribution of a wide resonance like the ρ. We write for the observed resonance production differential cross section[19]

$$\left.\frac{d\sigma}{dt}\right|_{\text{finite }\Gamma} = \int_{4m_\pi^2}^{\text{Max}M_{\pi\pi}^2(t)} dM_{\pi\pi}^2 f_{\text{res}}(M_{\pi\pi}) \frac{d\sigma_o}{dt}(M_{\pi\pi})$$

where $$f_{\text{res}}(M_{\pi\pi}) = \frac{\sin^2\delta(M_{\pi\pi})}{\pi M_{\text{res}}\Gamma(M_{\pi\pi})},$$

and $d\sigma_o/dt(M_{\pi\pi})$ is the cross section to produce the resonant $\pi\pi$ system in a state of mass $M_{\pi\pi}$. To first approximation $d\sigma_o/dt(M_{\pi\pi})$ does not vary over the width of the resonance and can therefore be replaced by $d\sigma/dt\big|_{\Gamma=0}$; thus

$$\left.\frac{d\sigma}{dt}\right|_{\text{finite }\Gamma} = \left.\frac{d\sigma}{dt}\right|_{\Gamma=0} \int_{4m_\pi^2}^{\text{Max}M_{\pi\pi}^2(t)} dM_{\pi\pi}^2 f_{\text{res}}(M_{\pi\pi}).$$

The t-dependent integral then gives the kinematic correction due to the finite width. Note that in calculating the total cross section

$$\sigma_{\Gamma=0} = \int_{|t|_{MIN}}^{|t|_{MAX}} \left.\frac{d\sigma}{dt}\right|_{\Gamma=0} dt \qquad (11)$$

for resonance production, the limits of integration are those calculated for the resonance mass.

The corrected differential cross sections $d\sigma/dt|_{\Gamma=0}$ for the reaction (1) are shown in fig.6. For the correction of the differential cross sections obtained with assumption (i), $f_{res}(M_{\pi\pi})$ was multiplied by a factor $(M_\rho/M_{\pi\pi})^4$. A fit of an exponential form

$$\left.\frac{d\sigma}{dt}\right|_{\Gamma=0} = A \exp(Bt)$$

to these differential cross sections gives values of A and B as shown in table 1. With the assumption that $d\sigma/dt$ is exponential throughout, the total cross section of reaction (1) corrected for the finite width effect can be calculated from equation (11). The result obtained does not depend on the assumed ρ^o resonance shape. As an average over the photon energy range $1.8 < E_\gamma < 5.3$ GeV we obtain $\sigma_{\Gamma=0}(\gamma d \to \rho^o d) = (13 \pm 2)$ μb.

3.14 ρ^o Decay

The decay angular distributions of the $\pi^+\pi^-$ systems in the ρ^o mass region and with cms production angles near the forward direction are shown in fig.7. Three different choices of the quantization axis $\hat{z}$ are used. In the helicity system $\hat{z}$ is parallel to the cms momentum of the ρ^o, while in the Gottfried-Jackson and Adair systems $\hat{z}$ is parallel to the photon momentum in the ρ^o rest frame or in the overall cms, respectively. From fits to these decay angular distributions the curves and the density matrix elements given in fig.7 were obtained. Figure 8 shows the t dependence of the density matrix elements ρ_{oo}, Re ρ_{1o} and ρ_{1-1}. Near the forward direction the helicity density matrix element ρ_{oo} is compatible with zero, i.e. with s-channel helicity conservation.

3.2 The Reaction $\gamma d \to \omega d$

In fig.9 the effective mass distribution of the three-pion system of all three-prong events fitting hypothesis (6), $\gamma d \to \pi^o\pi^+\pi^- d$, is shown (unshaded histogram). The kinematic range is restricted to $1.4 < E_\gamma < 5.3$ GeV and $0.05 < |t| < 0.20$ GeV^2. No clear ω enhancement is seen in the large background. This background can be reduced by using only events in the central region of the three pion Dalitz plot, since the density distribution for the decay of a $J^P = 1^-$ resonance into three pions has its maximum in the centre of the Dalitz plot[20]. The central region, which contains 50 % of all decays, can be defined in a mass independent way by

$$\frac{|\vec{p}_+ \times \vec{p}_-|^2}{(M^2(\pi^o\pi^+\pi^-) - 9m_\pi^2)^2} > 0.0065$$

where $\vec{p}_+$ and $\vec{p}_-$ are the momenta of the π^+ and π^- in the three-pion rest system[21] The shaded histogram in fig.9 shows the $M(\pi^o\pi^+\pi^-)$-distribution for this central region. A clear ω signal is now observed.

The fraction of ω production was determined by fitting to the shaded histogram of fig. 9 an incoherent superposition of a hand-drawn background and a non-relativistic Breit-Wigner folded with a mass resolution function of triangular shape[22] (full curve in fig. 9). The resonance parameters were fixed. The cross section thus obtained is $\sigma(\gamma d \to \omega d) = (0.64 \pm 0.17)$ µb for $1.4 < E_\gamma < 5.3$ GeV and $0.05 < |t| < 0.20$ GeV^2. This number is corrected for the unobserved ω decay modes.

3.3 The Reaction $\gamma n \to \rho^- p$

We now discuss the reactions (8), $\gamma n \to \pi^o\pi^- p$, and (3), $\gamma n \to \rho^- p$,[23,24] which are deduced from the reaction (7), $\gamma d \to \pi^o\pi^- pp_s$, by means of the spectator model. As appropriate energy variable we use the effective laboratory photon energy

$$E_\gamma^{eff} = (s - m_n^2)/(2m_n) \qquad (12)$$

where s is the square of the invariant mass of the $\pi^o\pi^- p$ system and m_n the on-shell neutron's mass. E_γ^{eff} is the photon energy required to give the cms energy $\sqrt{s}$ with an on-shell target neutron at rest.

3.31 Provisions for the Use of the Spectator Model

In order to determine cross sections on the neutron as target particle from our data, we have tried to select a subsample of events in which one of the protons can be approximately considered to be a spectator. We show in fig. 10 the distribution of the momentum $|\vec{p}_s|$ of the slower one of the two protons in reaction (7). The shaded area corresponds to the amount of invisible proton tracks ($|\vec{p}_s| \lesssim 0.1$ GeV/c). The events are weighted such as to unfold phase space and photon spectrum effects[7]. If all of the lower-energy protons were spectators, the distribution should agree with the Fermi momentum distribution in the deuteron which is shown for comparison, normalized to the observed number of events in the range $0 < |\vec{p}_s| < 0.2$ GeV/c. It has been calculated from a modified Hamada-Johnston wave function[25] in the parametrization of J. Humberston which is quoted in ref. 26. Approximate agreement between the data and the theoretical distribution is observed for $|\vec{p}_s| < 0.2$ GeV/c, but clear deviations occur at higher $|\vec{p}_s|$.

To check further whether protons with $|\vec{p}_s| < 0.2$ GeV/c can be considered to be spectators to sufficient accuracy, we study the distribution of the Treiman-Yang angle φ_T for these protons[27,28]. This angle is defined as the azimuthal angle of $\vec{p}_s$ in the rest frame of the photon and the exchanged neutron, i.e.

$$\cos\varphi_T = \frac{\vec{p}_d \times \vec{p}_s}{|\vec{p}_d \times \vec{p}_s|} \cdot \frac{\vec{p}_{\pi o} \times \vec{p}_\gamma}{|\vec{p}_{\pi o} \times \vec{p}_\gamma|}$$

Instead of $\vec{p}_{\pi o}$, also the momentum vector of the π^- or of the faster proton can be used to define the plane $\varphi_T = 0$. In all cases these distributions must be flat if a single neutron is exchanged as the spectator picture assumes. This can be checked for three-prong events (i.e. events with a visible spectator) and is fulfilled (fig. 11).

Therefore, we consider the subsample of events with $|\vec{p}_s| < 0.2$ GeV/c as a sample of photon reactions on a target of quasi-free off-mass-shell neutrons. The calculation of cross sections in the spectator model proceeds as in ref.7. All cross sections are then raised by 22 %, in order to correct for the restriction in the spectator momentum. This correction was determined from the fraction of events with $|\vec{p}_s| > 0.2$ GeV/c. Possible effects of the Pauli exclusion principle on the two final state protons, of multiple scattering and

of shadowing cannot be calculated since the phase and spin dependence of the amplitude are not known. There are 4933 events assigned to reaction (7) after the acceptance cuts in t (see section 2.3) and $|\vec{p}_s|$ are made. Among these events, 1788 have $E_\gamma^{eff} > 1.1$ GeV, i.e. are above the rho production threshold.

3.32 Cross Section for the Reaction $\gamma n \to \pi^o \pi^- p$

Fig. 12 shows the total cross section of the reaction (8) for E_γ^{eff} between threshold and 5 GeV (black dots). Corrections for multiple π^o events have been applied (see below). No cut in $t = (p_\gamma - p_{\pi\pi})^2$ is made. The background from other reactions with the same number of charged particles (see section 2.3) was estimated from the results of that part of our experiment which was done with a tagged photon beam[6] and the contribution of this background to the total cross section of reaction (8) has been subtracted. This correction is important for $E_\gamma^{eff} > 1.2$ GeV only. The results of the FNPR collaboration[29] (open circles) and the Weizmann group[4] (diamonds) are also shown in fig.12. They are compatible with our data.

3.33 ρ^- Production

The effective mass distributions of the $\pi^o\pi^-$, $\pi^o p$ and $\pi^- p$ systems from reaction (8) are shown in figs.13a-c for various intervals of E_γ^{eff} between 1.1 and 5.3 GeV. The t-range is restricted to $|t| < 1.1$ GeV^2. Production of ρ^-, $\Delta^+(1236)$ and $\Delta^o(1236)$ is observed.

For a more detailed study of the reaction (3) we had to estimate the amount and distribution of the background from multiple π^o production (see section 2.3). This was done starting from "all charged" reactions like $\gamma n \to \pi^- \rho^o p$ and $\gamma n \to \pi^-\pi^+\pi^- p$ which can be completely separated from background. We assumed that the reactions $\gamma n \to \pi^o \rho^- p$ and $\gamma n \to \pi^o\pi^o\pi^- p$, which contribute the bulk of the background to reactions (3) and (8), have similar mass distributions as the "all charged" reactions, and that their total cross sections can be estimated from the "all charged" reactions by assuming statistical weighting of the isospin states[30,31]. We then studied how the photon energy E_γ and the other calculated kinematical variables get changed if a single π^o is substituted for the two π^o's. In this way the background in the various distributions was

evaluated. It was found that depending on the kinematics part of the reaction $\gamma n \to \pi^o \rho^- p$ is indistinguishable from the reaction $\gamma n \to \rho^- p$. This background was therefore always subtracted from our ρ^- cross sections. For differential cross sections the hypothesis of statistical mixing of the isospin states appears to be too uncertain to be applied directly; therefore our values of $d\sigma/dt(\gamma n \to \rho^- p)$ may be affected by some background from the reaction $\gamma n \to \pi^o \rho^- p$.

The fraction of ρ^- production was determined by fits assuming ρ^-, Δ^+ and Δ^o production as well as a phase space background (curves in fig. 13). To take account of finite resolution effects and systematic shifts in the $\pi^o\pi^-$ mass distribution (see section 2.3 and ref. 5), the width of the ρ^- was fixed at $\Gamma_{\rho^-} = 0.180$ GeV and its mass was taken as a free parameter.

3.34 Total and differential Cross Sections for the Reaction $\gamma n \to \rho^- p$.

The cross section $\sigma(\gamma n \to \rho^- p)$ for $|t| < 1.1$ GeV^2 obtained from these fits and corrected for multiple π^o events is shown in fig. 14 as a function of E_γ^{eff} (black dots). The cross section increases from threshold to a maximum value of about 7 μb at $E_\gamma^{eff} \approx 1.6$ GeV ($\sqrt{s} \approx 2$ GeV) and slowly decreases at higher energies. The result of the Weizmann group[4] (diamond) is also shown in fig. 14. It agrees with our data.

The differential cross sections $d\sigma/dt(\gamma n \to \rho^- p)$ were determined by repeating the fits independently in various t intervals. They are shown in fig. 15 for the E_γ^{eff} range 1.2 to 2.5 GeV. The first point at $|t| = 0.084$ GeV^2 is corrected by +20 % for kinematic inaccessibilities due to the mass dependence of the minimum momentum transfer. The t dependence of the differential cross section is weak. The dashed line shows an exponential with a slope of 1.9 GeV^{-2}.

4. Discussion of the Results

4.1 Determination of the Coupling Constant Ratio $g^2_{\gamma\omega}/g^2_{\gamma\rho}$

In the framework of the vector dominance model and of the additive quark model for elastic ρ^o and ω scattering the cross section ratio for ω and ρ^o production on deuterons should be equal to the squared ratio of the $\gamma\omega$ and $\gamma\rho$ coupling constants. SU(3) with ideal $\omega\Phi$ mixing gives the well-known result $g^2_{\gamma\omega}:g^2_{\gamma\rho} = 1:9$, but various symmetry-breaking schemes lead to slightly modified predictions: $(0.65 : 9)$[32] or $(1.21 : 9)$[33]. The ρ^o cross section (obtained by assumption (i) on the resonance shape and corrected for the finite ρ^o width, see section 3.1) is $\sigma(\gamma d \to \rho^o d) = (4.6 \pm 0.4)$ µb for $1.4 < E_\gamma < 5.3$ GeV and $0.05 < |t| < 0.20$ GeV^2. Thus, with our result for $\sigma(\gamma d \to \omega d)$ (section 3.2), we find

$$\frac{g^2_{\gamma\omega}}{g^2_{\gamma\rho}} = \frac{\sigma(\gamma d \to \omega d)}{\sigma(\gamma d \to \rho^o d)} = 0.14 \pm 0.04 = (1.26 \pm 0.36) : 9$$

The experimental value for this ratio is less sensitive to scanning bias and normalization uncertainties than each cross section itself. The Weizmann group[4] found $g^2_{\gamma\omega}/g^2_{\gamma\rho} = 0.15 \pm 0.07$ from their ρ^o and ω production data on deuterons at $E_\gamma = 4.3$ GeV. Both their and our values are in good agreement with the result $g^2_{\gamma\omega}/g^2_{\gamma\rho} = 0.14 \pm 0.02 = (1.26 \pm 0.18) : 9$ from e^+e^- colliding beam experiments at Orsay[34]. All of these results agree best with the prediction of ref. 33.

4.2 Isospin Analysis of the ρ^o Photoproduction Amplitude

4.21 Comparison of ρ^o Production on Protons and Deuterons

Starting from our measured data[35] on the reaction $\gamma p \to \rho^o p$, we have calculated the expected differential cross section for coherent ρ^o production on the deuteron (reaction (1)). In this calculation[3] we used the second order impulse approximation and also took the effects of the Fermi motion into account. Since our $\gamma d \to \rho^o d$ data are at a rather small $|t|$, the dominating term in the amplitude is the single scattering term. In the limit that effects of the Fermi motion are relatively unimportant at our energies, the single scattering

amplitude is proportional to the sum

$$T(\gamma p \to \rho^o p) + T(\gamma n \to \rho^o n) = 2T_o$$

of the ρ^o production amplitudes on protons and neutrons, i.e. proportional to the I = 0 exchange amplitude T_o on single nucleons, because the I = 1 exchange amplitude T_1 has different signs on protons and neutrons. Thus, the differential cross section $d\sigma/dt(\gamma d \to \rho^o d)$ is essentially proportional to $|T_0|^2$ while the differential cross section for ρ^o production on protons is proportional to $|T_0 + T_1|^2$.

In the calculation of the amplitude of reaction (1) we assumed T_0 to be helicity conserving and mainly imaginary, i.e. $ReT_0/ImT_0 = -0.20$.[36,37] The phase of T_0 enters in the interference between single and double scattering, but due to the smallness of the latter the dependence of the cross section on the phase is not at all critical. Double scattering in the deuteron causes a decrease of the cross section by about 9 % in our E_γ and t region; the elastic $\rho^o N$ scattering amplitudes that enter in the double scattering calculation were derived from the SLAC measurements in the double scattering region[2] which are consistent with the ρ^o photoproduction data on complex nuclei and also with the quark and vector dominance models.

Since we do not know $|T_0|^2$, we made an approximate calculation of $d\sigma/dt(\gamma d \to \rho^o d)$ in which we replaced $|T_0|^2$ by $|T_0 + T_1|^2$ as obtained from our measured data[35] on $d\sigma/dt(\gamma p \to \rho^o p)$. By comparison with the measured $d\sigma/dt(\gamma d \to \rho^o d)$ we thus obtain the ratio

$$R \equiv \frac{d\sigma/dt(\gamma d \to \rho^o d)_{calculated}}{d\sigma/dt(\gamma d \to \rho^o d)_{measured}} \approx \frac{|T_0 + T_1|^2}{|T_0|^2} = 1 + \frac{|T_1|}{|T_0|} 2\cos\Delta\Phi + \frac{|T_1|^2}{|T_0|^2}, \qquad (13)$$

where $\Delta\Phi$ is the relative phase of T_0 and T_1. In fig. 5 the comparison between the calculated and the measured $d\sigma/dt(\gamma d \to \rho^o d)$ is made, and good agreement is found throughout the E_γ and t range measured. The calculated cross sections integrated over t and the corresponding values of R are given in table 2 for the t range $0.04 < |t| < 0.20$ GeV^2. The R values are consistent with one within 10 %.

Not much is known about $\Delta\Phi$, except that it can be shown[38] to lie outside the range $90^o \pm \psi$ where $(90^o + \psi)$ is the absolute phase angle of T_0. ψ has

been experimentally determined[36,37] to be approximately 12° to 16°. Thus, $|\cos\Delta\Phi| \gtrsim 0.2$. Unfortunately the paucity of the data precludes any conclusion on the size of $|T_1/T_0|$ if $\cos\Delta\Phi < 0$. On the other hand, if $\cos\Delta\Phi > 0$, from equation (13) and our values of R it follows that $|T_1/T_0| < 0.3$ within one standard deviation for the energy range $1.8 < E_\gamma < 5.3$ GeV. Further information on $|T_1/T_0|$ will be derived in the next section.

4.22 Comparison of ρ^- Production on Neutrons with ρ^0 Production on Protons

The full curves in figs. 14 and 15 show the pion exchange (OPE) cross section[39] for ρ^- production, using $\Gamma_{\rho\pi\gamma} = \frac{1}{9}\Gamma_{\omega\pi\gamma} = 0.13$ MeV as expected from SU(3) and the quark model. It is compatibel with the data for $E_\gamma^{eff} > 2.5$ GeV but fails at lower energies. The difference between the data and the OPE prediction may be partly due to ρ^- exchange. Calculations of its contribution[40] are very sensitive to the value of the magnetic moment of the ρ and are too uncertain up to now to draw further conclusions.

Also shown in fig. 14 is the qualitative behaviour of $\sigma(\gamma p \to \rho^0 p)$. For $E_\gamma^{eff} > 3$ GeV the ρ^- cross section is less than 1/10 of the ρ^0 cross section and even in the low energy region ρ^- production is not stronger than about 1/3 of ρ^0 production, i.e. I = 0 exchange (P,P') obviously dominates in ρ^0 production also at low energies. The measurement of $\sigma(\gamma n \to \rho^- p)$ allows to further investigate the contribution of I = 1 exchange to ρ^0 production on nucleons. Principal exchanges are

$$P, P', \pi^0, A_2^0 \quad \text{for} \quad \gamma p \to \rho^0 p$$

$$\text{and} \quad \pi^-, \rho^-, A_2^- \quad \text{for} \quad \gamma n \to \rho^- p \ .$$

At high energies the exchange contribution of π and ρ or π and A_2 do not interfere[41] and if one assumes that ρ^- and A_2^- exchange in ρ^- production do not essentially cancel one can estimate the I = 1 exchange contribution by

$$\sigma(\gamma p \to \rho^0 p)^{(\pi^0 + A_2^0)} \lesssim \frac{1}{2}\sigma(\gamma n \to \rho^- p)^{(\pi^- + \rho^- + A_2^-)} = \frac{1}{2}(1.0 \pm 0.5)\ \mu b$$

for $E_\gamma^{eff} > 3.5$ GeV. Thus for ρ^0 production one finds

$$\frac{\sigma(\gamma p \to \rho^0 p)^{(I=1\ \text{exchange})}}{\sigma(\gamma p \to \rho^0 p)^{\text{total}}} \lesssim 5\ \%$$

within one standard deviation, which however still allows 30 (20)% in amplitude for $\cos\Delta\Phi > 0$ (<0), where $\Delta\Phi$ is the relative phase of the I = 0 and I = 1 exchange amplitudes. This is consistent with the results from the previous section. It is also consistent with the small contribution from π^o exchange found by the SBT collaboration[42] in ρ^o production. At E_γ = 4.7 GeV they found $\sigma^U(\gamma p \to \rho^o p)/\sigma^{tot}(\gamma p \to \rho^o p) = (-1.1 \pm 2.8)\%$, where σ^U is the unnatural parity exchange cross section.

4.23 Isospin of the s-Channel Peaks in ρ^o and ρ^- Photoproduction

In the s-channel picture the peak of the ρ^- cross section at $\sqrt{s} \approx 2$ GeV may be due to excitation of s-channel resonances via $\gamma n \to$ (N or Δ (~2 GeV))$\to \rho^- p$. A rough estimate of their formation cross section from fig. 14 gives 6 μb (after subtraction of the OPE contribution), i.e. approximately half of that for ρ^o production assuming a diffractive background of about 15 μb there. A ratio of $\sigma(\gamma n \to (N \text{ or } \Delta) \to \rho^- p) : \sigma(\gamma p \to (N \text{ or } \Delta) \to \rho^o p) = 1 : 2$ favoures the dominance of I = 3/2 resonances, whereas for the excitation of I = 1/2 resonances the ratio would be 2 : 1. Possible candidates are the F35(1890), P31(1910) and F37(1950). From the measured γN and ρN decay widths[43] of these Δ resonances, one expects their contributions to the reaction $\gamma n \to \Delta \to \rho^- p$ to be ~1.8 μb, ~0.1 μb and ~1.7 μb respectively at the resonance energies.

4.3 Isospin Analysis of the ω Photoproduction Amplitude

An interesting question is the amount of A_2 exchange to ω production on protons. From the observed difference of the total photon cross sections on neutrons and protons, Harari[44] has predicted a large contribution from A_2 exchange in the reaction $\gamma p \to \omega p$. It is given by the relation

$$\frac{\text{Im } T^1 \ (\gamma p \to \omega p)}{\text{Im } T^0 \ (\gamma p \to \omega p)} \approx \frac{1}{2} \left(\frac{g_{\gamma\rho}}{g_{\gamma\omega}}\right)^2 \frac{\sigma_{tot}(\gamma p) - \sigma_{tot}(\gamma n)}{\sigma_{tot}(\gamma p) + \sigma_{tot}(\gamma n)} \qquad (14)$$

where T^0 and T^1 are the forward amplitudes for isoscalar (P and P') and isovector (A_2) exchange, respectively (the contribution of pion exchange vanishes in the forward direction). In the photon energy range 2 to 4 GeV a NINA group[45] has measured an average value of $\sigma_{tot}(\gamma n)/\sigma_{tot}(\gamma p) = 0.94 \pm 0.01$. Together with

the Orsay measurements[34] of $g^2_{\gamma\omega}/g^2_{\gamma\rho}$ one finds 0.110 ± 0.025 for the right hand side of equation (14), which allows a 20 % contribution of A_2 exchange plus interference terms to the natural parity exchange cross section $d\sigma^N/dt(\gamma p \to \omega p)$ at t = 0.

Measurements of coherent ω production on deuterons provide an independent way to determine the A_2 exchange contribution. Since only I = 0 exchange is allowed here, one has, neglecting Glauber corrections,

$$\left.\frac{d\sigma/dt\ (\gamma d \to \omega d)}{d\sigma^N/dt(\gamma p \to \omega p)}\right|_{t=0} = \frac{4|T^0|^2}{|T^0+T^1|^2} \qquad (15)$$

The forward cross section for coherent ω production can be calculated from $d\sigma/dt(\gamma d \to \rho^o d)$ (Γ_ρ = 0) and the ω-ρ^o cross section ratio, if one assumes that coherent ω and ρ^o production have the same slope; then $d\sigma/dt(\gamma d \to \omega d)$ = = (57 ± 19)μb/GeV^2 at t = 0. The forward cross section for ω production on protons via natural parity exchange has been measured by the SBT collaboration[46]. At E_γ = 2.8 (4.7) GeV they found $d\sigma^N/dt(\gamma p \to \omega p)$ = 14.5 ± 5.1 (14.6 ± 4.8)μb/GeV^2 at t = 0. Using this for the left hand side of equation (15) we find 3.9 ± 1.8, which gives a contribution of A_2 exchange plus interference of (+2 ± 45)%, consistent with the result from the total cross section measurements.

4.4 Test of Duality and Regge Factorization

Roberts and Roy[47] have noted that semi-local Harari-Freund duality and factorization of Regge exchange provide a simple way to relate pion and photon induced reactions. For the pion exchange contributions to the reactions $\pi^- p \to \rho^o n$ and $\gamma n \to \rho^- p$ one predicts

$$\frac{\sigma^{(\pi)}(\gamma n \to \rho^- p)}{\sigma^{(\pi)}(\pi^- p \to \rho^o n)} = \frac{1}{2}\frac{\beta_{P'\gamma\gamma}}{\beta_{P'\pi\pi}} \qquad (16)$$

where $\beta_{P'\pi\pi}$ and $\beta_{P'\gamma\gamma}$ are the ππ and the γγ couplings of the leading trajectory P' in resonant ππ and γπ scattering. The right hand side of equation (16) can be evaluated from Regge analysis of the total πN and γN cross sections to be 0.0023. The reaction $\pi^- p \to \rho^o n$ is expected to be dominated by pion exchange and its cross section at 4.3 GeV beam momentum is about 750 μb.[48] For

the pion exchange contribution in $\gamma n \to \rho^- p$ we can give the upper limit $\sigma^{(\pi)}(\gamma n \to \rho^- p) \leq \sigma(\gamma n \to \rho^- p) = (1.0 \pm 0.5)$ μb for $E_\gamma^{eff} > 3.5$ GeV, and thus the left hand side of equation (16) is

$$\frac{\sigma^{(\pi)}(\gamma n \to \rho^- p)}{\sigma^{(\pi)}(\pi^- p \to \rho^0 n)} \leq 0.0013 \pm 0.0007,$$ i.e. still barely compatible with the semi-local factorization prediction.

Acknowledgements

We thank M.W. Teucher and E. Lohrmann for their interest and encouragement, H. Meyer and H. Spitzer for their participation in the early stages of this experiment, and G. Horlitz and S. Wolff for an efficient run of the bubble chamber. This work was supported by the Bundesministerium für Forschung und Technologie.

References

1. G. McClellan et al., Phys. Rev. Letters 22 (1969) 374
2. R.L. Anderson et al., Phys. Rev. D4 (1971) 3245
3. H.G. Hilpert et al., Aachen-Bonn-Hamburg-Heidelberg-München Collaboration, Nucl. Phys. B23 (1970) 45
4. Y. Eisenberg et al., Nucl. Phys. B42 (1972) 349
5. H.G. Hilpert et al., Aachen-Bonn-Hamburg-Heidelberg-München Collaboration, Nucl. Phys. B21 (1970) 93
6. R. Schiffer et al., Aachen-Bonn-Hamburg-Heidelberg-München Collaboration, Nucl. Phys. B38 (1972) 628
7. P. Benz et al., Aachen-Bonn-Hamburg-Heidelberg-München Collaboration, Nucl. Phys. B65 (1973) 158
8. CERN program library, X-601, unpublished
9. D. Gall, Diplomarbeit, Hamburg 1971, unpublished
10. J. Ballam et al., Phys. Rev. Letters 24 (1970) 955
11. S.D. Drell, Phys. Rev. Letters 5 (1960) 278
12. P. Söding, Phys. Letters 19 (1966) 702
13. A.S. Krass, Phys. Rev. 159 (1967) 1496
14. V. Franco and R.J. Glauber, Phys. Rev. 142 (1966) 1195
15. J. Pumplin, Phys. Rev. D2 (1970) 1859
16. T. Bauer, Phys. Rev. Letters 25 (1970) 485
17. D.R. Yennie, Proc. of the 11th session of the Scottish Universities Summer School in Physics 1970, ed. J. Cummings and H. Osborn (1971),p.321
18. F. Gutbrod, private communication
19. J.D. Jackson, Nuovo Cimento 34 (1964) 1644
20. C. Zeemach, Phys. Rev. 133B (1964) 1201
21. M.S. Rabin et al., Phys. Rev. Letters 24 (1970) 925
22. D.G. Coyne et al., Nucl. Phys. B32 (1971) 333
23. U. Idschok, Thesis, Bonn Univ. PIB 3-21 (1972), unpublished
24. F. Storim, Thesis, internal report DESY F1-73/1 (1973), unpublished
25. T. Hamada and I.D. Johnston, Nucl. Phys. 34 (1962) 382
26. C. Michael and C. Wilkin, Nucl. Phys. B11 (1969) 99
27. S.B. Treiman and C.N. Yang, Phys. Rev. Letters 8 (1962) 140
28. L.I. Gutay et al., Phys. Letters 16 (1965) 343
29. A. Piazza et al., Lettere al Nuovo Cimento 3 (1970) 403

30. J. Shapiro, Nuovo Cimento Suppl. 18 (1960) 40
31. H. Satz, Phys. Letters 25B (1967) 27; Phys. Rev. Letters 19 (1967) 1453
32. R.J. Oakes and J.J. Sakurai, Phys. Rev. Letters 19 (1967) 1266
33. T. Das, V.S. Mathur and S. Okubo, Phys. Rev. Letters 19 (1967) 470
34. D. Benaksas et al., Phys. Letters 39B (1972) 289;
D. Benaksas et al., Phys. Letters 42B (1972) 507
35. Aachen-Berlin-Bonn-Hamburg-Heidelberg-München Collaboration, Phys. Rev. 175 (1968) 1669
36. H. Alvensleben et al., Phys. Rev. Letters 25 (1970) 1377
37. P.J. Biggs et al., Phys. Rev. Letters 27 (1971) 1157
38. D. Julius, Nucl. Phys. B33 (1971) 558
39. G. Wolf, SLAC-PUB-544 and private communication
40. N. Levy, M. Glück and S. Wagner, Phys. Rev. D4 (1971) 874
41. K. Schilling, P. Seyboth and G. Wolf, Nucl. Phys. B15 (1970) 397
42. J. Ballam et al., Phys. Rev. D5 (1972) 545
43. Particle Data Group, Review of Particle Properties, Review of Mod. Physics 45 (1973) No.2, Part II
44. H. Harari, Proceedings of the 4th International Symposium on Electron and Photon Interactions at High Energies, Liverpool 1969, p.107
45. T.A. Armstrong et al., Nucl. Phys. B41 (1972) 445
46. J. Ballam et al., Phys. Rev. D7 (1973) 3150
47. R.G. Roberts and D.P. Roy, Phys. Letters 47B (1973) 247
48. E. Bracci et al., CERN/HERA 72-1 (1972)

Table 1: Results of fitting an exponential A exp(Bt) to the differential cross sections $d\sigma/dt\big|_{\Gamma=0}$ (corrected for finite width effects) for coherent ρ^o production, $\gamma d \to \rho^o d$, in the t range $0.04 < |t| < 0.20$ GeV^2. The model assumptions are explained in section 3.12.

E_γ (GeV)	1.8 - 2.5	2.5 - 3.5	3.5 - 5.3	1.8 - 5.3	model
A (μb GeV^{-2})	467 ± 144	541 ± 148	335 ± 77	410 ± 67	assumption
B (GeV^{-2})	25.5 ± 3.9	29.5 ± 3.2	24.2 ± 2.5	25.5 ± 1.8	(i)
A (μb GeV^{-2})	468 ± 108	470 ± 120	312 ± 75	383 ± 60	assumption
B (GeV^{-2})	23.8 ± 2.7	26.5 ± 3.1	22.6 ± 2.8	23.7 ± 1.8	(ii)
A (μb GeV^{-2})	481 ± 111	502 ± 129	327 ± 83	402 ± 65	assumption
B (GeV^{-2})	24.0 ± 2.7	26.9 ± 3.2	22.9 ± 2.9	24.0 ± 1.8	(iii)

Table 2: Total cross sections for $\gamma d \to \rho^o d$ in the t range $0.04 < |t| < 0.20$ GeV^2

E_γ (GeV)	$\sigma(\mu b)^*$ observed	$\sigma(\mu b)^{**}$ calculated	R
1.8 - 2.5	6.3 ± 0.8	6.0	0.95 ± 0.15
2.5 - 3.5	5.3 ± 0.7	5.7	1.08 ± 0.18
3.5 - 5.3	4.9 ± 0.7	5.4	1.10 ± 0.20
1.8 - 5.3	5.3 ± 0.5	5.6	1.06 ± 0.15

* Obtained with assumption (i) on the resonance shape (see section 3.12).

** The calculated cross sections have uncertainties of about 10 % which come both from the errors of the input data and from approximations in the calculation.

Figure Captions

Fig. 1 Pulls for three-prong events of the reaction $\gamma d \to \pi^+\pi^- d$. p is the momentum, λ the dip angle and φ the azimuthal angle of the track with respect to the optical axis.

Fig. 2 Distribution of the laboratory break-up angle between the proton and the neutron for three-prong events of the reaction $\gamma d \to \pi^+\pi^- pn$, which are not ambiguous with the reaction $\gamma d \to \pi^+\pi^- d$.

Fig. 3 a-c Effective mass distributions of the $\pi^+\pi^-$, $\pi^+ d$ and $\pi^- d$ systems in the reaction $\gamma d \to \pi^+\pi^- d$ for the t range $0.04 < |t| < 0.2$ GeV^2 and various intervals of E_γ. The full (dashed) curves show the total (background) distribution obtained by fits using assumption (i) on the resonance shape (see section 3.12).

Fig. 4 a) Cross section of the reaction $\gamma d \to \pi^+\pi^- d$ as a function of E_γ for the t range $0.04 < |t| < 0.2$ GeV^2.

b) Cross section of the reaction $\gamma d \to \rho^o d$ as a function of E_γ for the t range $0.04 < |t| < 0.2$ GeV^2. The values are obtained by fits using assumption (i) (black dots), (ii) (open circles) and (iii) (open squares) on the resonance shape (see section 3.12).

Fig. 5 Differential cross sections of the reaction $\gamma d \to \rho^o d$. The values are obtained by fits using assumption (i) (black dots) and (ii) (open circles) on the resonance shape (see section 3.12). Also shown are the results of the Weizmann group[4] (diamonds) at $E_\gamma = 4.3$ GeV. The curves are predictions from the reaction $\gamma p \to \rho^o p$ assuming equal ρ^o photoproduction amplitudes on the proton and the neutron.

Fig. 6 Differential cross sections of the reaction $\gamma d \to \rho^o d$ after correcting for the finite width of the ρ^o (section 3.13). The symbols are the same as defined in fig. 5. The lines are obtained from a fit of an exponential to the data (assumption (ii)).

Fig. 7 Decay angular distributions of the $\pi^+\pi^-$ system for events of the reaction $\gamma d \to \pi^+\pi^- d$ with $M(\pi^+\pi^-)$ in the ρ^o mass region and cms production angles of the $\pi^+\pi^-$ system near the forward direction. The coordinate systems are defined in section 3.14. The curves are obtained from fits of the ρ^o density matrix elements.

Fig. 8 ρ^o density matrix elements as a function of t. The coordinate systems are defined in section 3.14.

Fig. 9 Distribution of the effective $\pi^o\pi^+\pi^-$ mass for three-prong events of the reaction $\gamma d \to \pi^o\pi^+\pi^- d$ in the kinematic region $1.4 < E_\gamma < 5.3$ GeV and $0.05 < |t| < 0.20$ GeV^2 (unshaded histogram). The distribution of the events in the central region of the Dalitz plot (see section 3.2) is shown by the shaded histogram. The curve is obtained by a fit of ω and background contributions.

Fig.10 Laboratory momentum distribution of the lower-energy proton in the reaction $\gamma d \to \pi^o\pi^- pp$. Each event is weighted such as to unfold phase space and photon spectrum effects[7]. The solid curve is the Fermi momentum distribution calculated from the deuteron wave function[25,26] and normalized to the observed number of weighted events with $|\vec{p}_s| < 0.2$ GeV/c.

Fig.11 Treiman-Yang angular distributions for the π^o, π^- and the higher-energy proton in the reaction $\gamma d \to \pi^o\pi^- pp$.

Fig.12 Total cross section of the reaction $\gamma n \to \pi^o\pi^- p$ as a function of E_γ^{eff}. The black dots are our data, the open circles (diamonds) are taken from ref. 29 (ref.4).

Fig.13 a-c Effective mass distributions of the $\pi^o\pi^-$, $\pi^o p$ and $\pi^- p$ systems in the reaction $\gamma n \to \pi^o\pi^- p$ (deduced from the reaction $\gamma d \to \pi^o\pi^- pp_s$) for $|t| < 1.1$ GeV^2 and various intervals of E_γ^{eff}. The curves are obtained from fits taking account of ρ^-, Δ^+, Δ^o and phase space contributions.

Fig.14 Total cross section of the reaction $\gamma n \to \rho^- p$ with the restriction $|t| < 1.1$ GeV^2 as a function of E_γ^{eff} (black dots). Also shown is the result of the Weizmann group[4] (diamond). The full curve shows the pion exchange prediction for $\gamma n \to \rho^- p$, the dashed curve shows the qualitative energy behaviour of $\sigma(\gamma p \to \rho^o p)$.

Fig.15 Differential cross section for the reaction $\gamma n \to \rho^- p$ in the E_γ^{eff} interval $1.2 < E_\gamma^{eff} < 2.5$ GeV. The first point at $t = 0.084$ GeV^2 is corrected for kinematic limits (see section 3.34). The full curves show the pion exchange prediction. The dashed line shows an exponential with a slope of 1.9 GeV^{-2}.

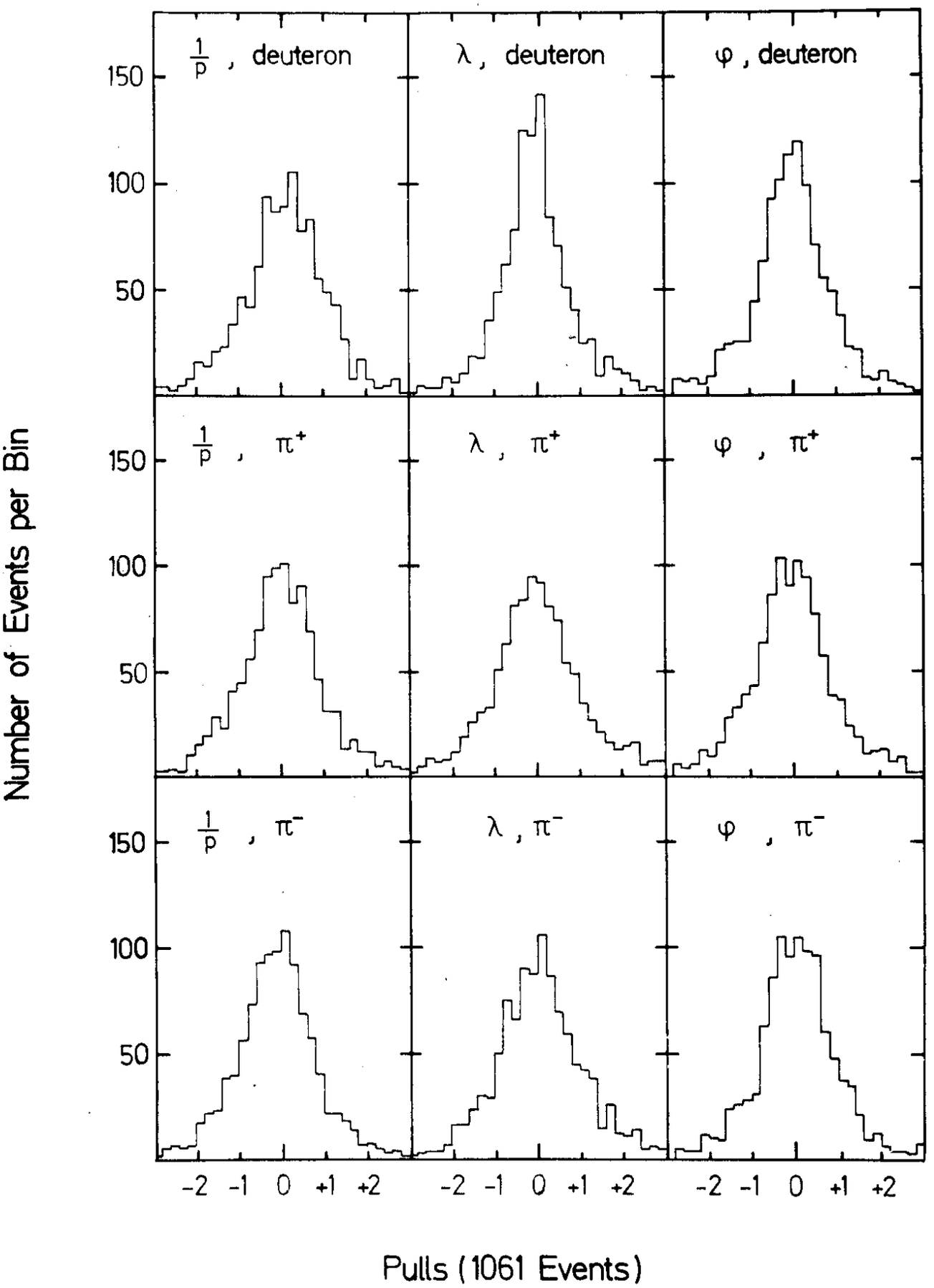
1/p , deuteron
λ , deuteron
φ , deuteron
1/p , π+
λ , π+
φ , π+
1/p , π−
λ , π−
φ , π−
150
100
50
-2 -1 0 +1 +2
Number of Events per Bin
Pulls (1061 Events)

Fig.1

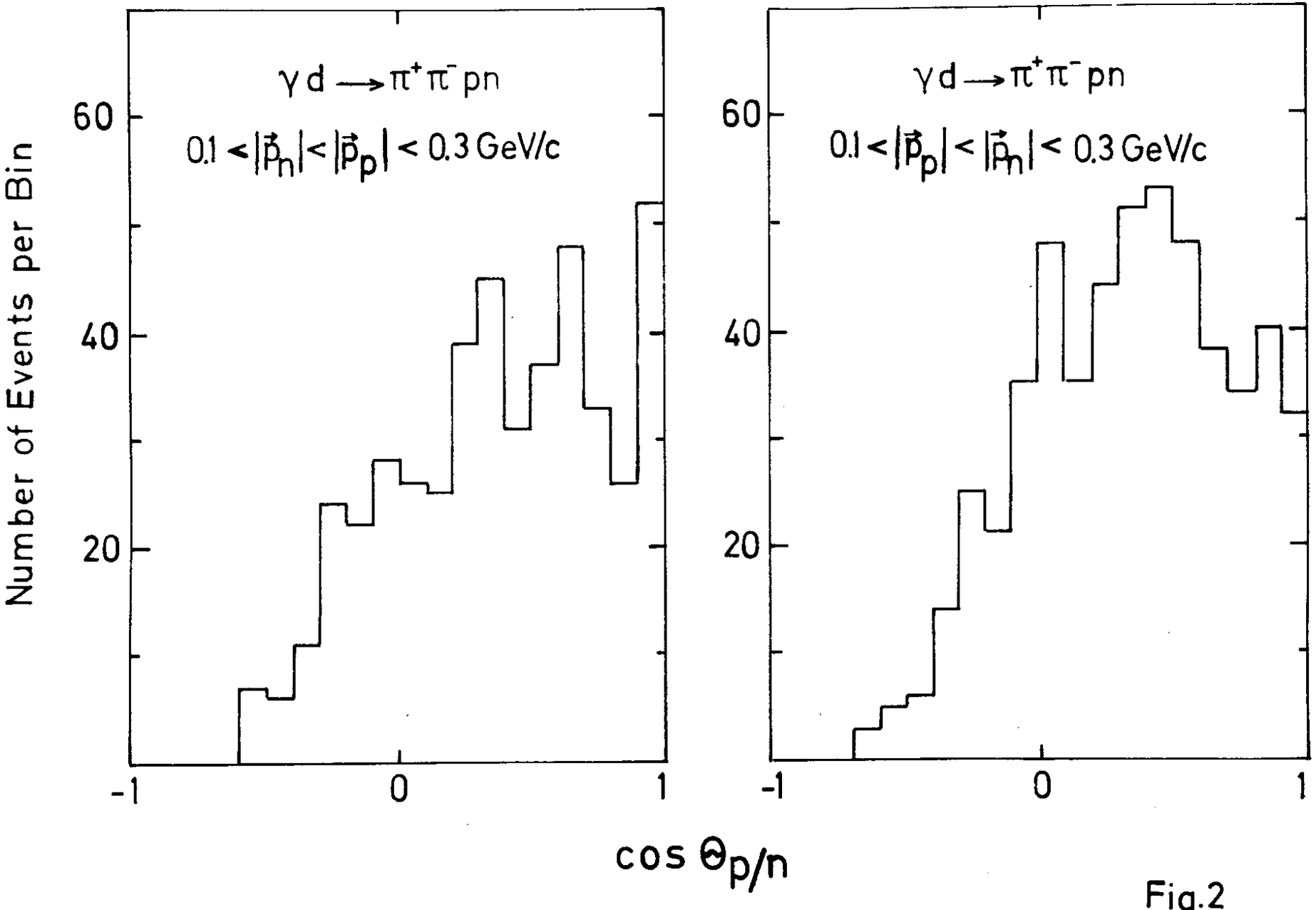
γ d → π⁺ π⁻ pn
0.1 < |p⃗n| < |p⃗p| < 0.3 GeV/c
γ d → π⁺ π⁻ pn
0.1 < |p⃗p| < |p⃗n| < 0.3 GeV/c
Number of Events per Bin
60
40
20
-1
0
1
cos Θp/n

Fig.2

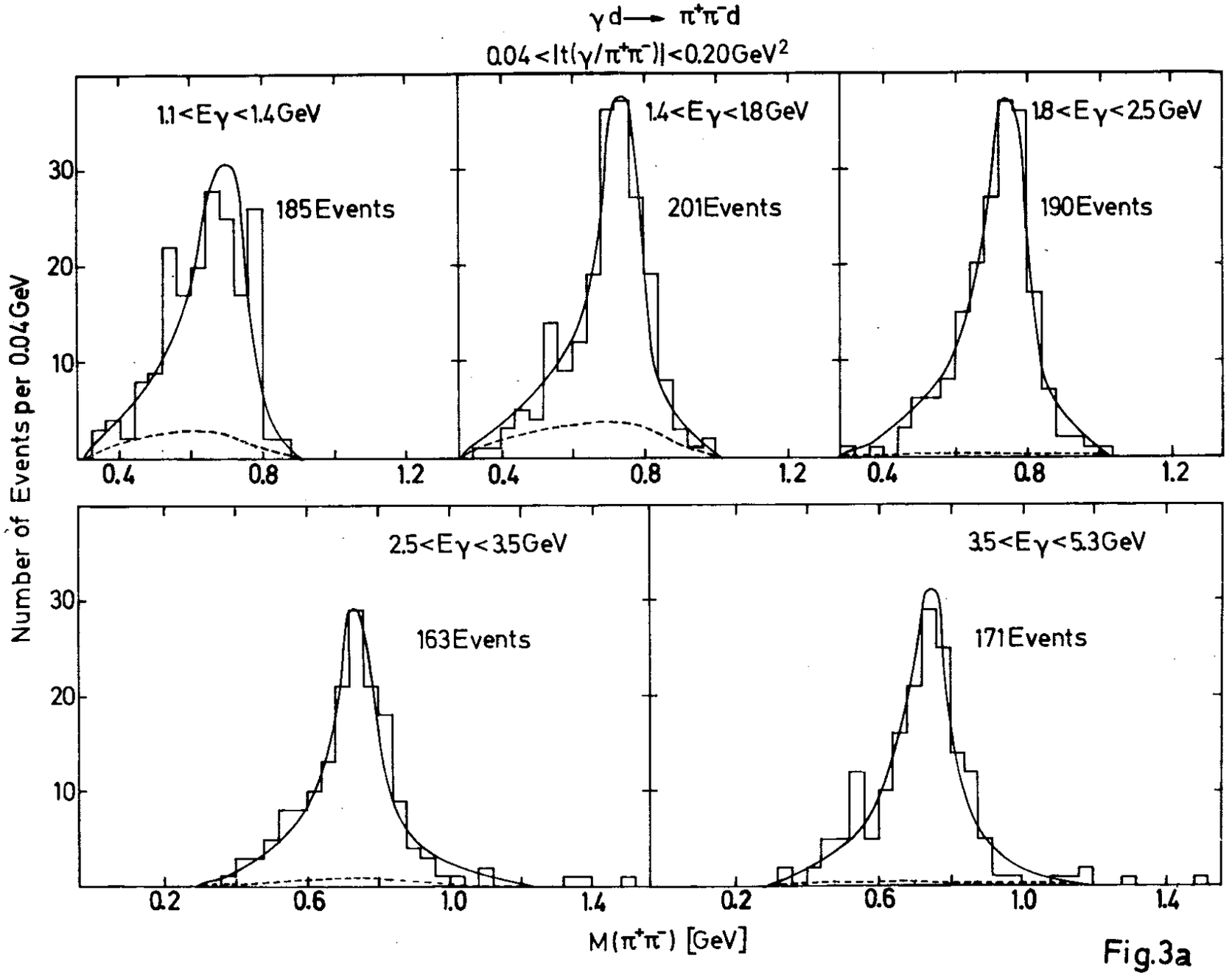
γ d⟶ π⁺π⁻d
0.04<|t(γ/π⁺π⁻)|<0.20GeV²
1.1<Eγ<1.4GeV
185Events
1.4<Eγ<1.8GeV
201Events
1.8<Eγ<2.5GeV
190Events
2.5<Eγ<3.5GeV
163Events
3.5<Eγ<5.3GeV
171Events
Number of Events per 0.04GeV
M(π⁺π⁻) [GeV]

Fig.3a

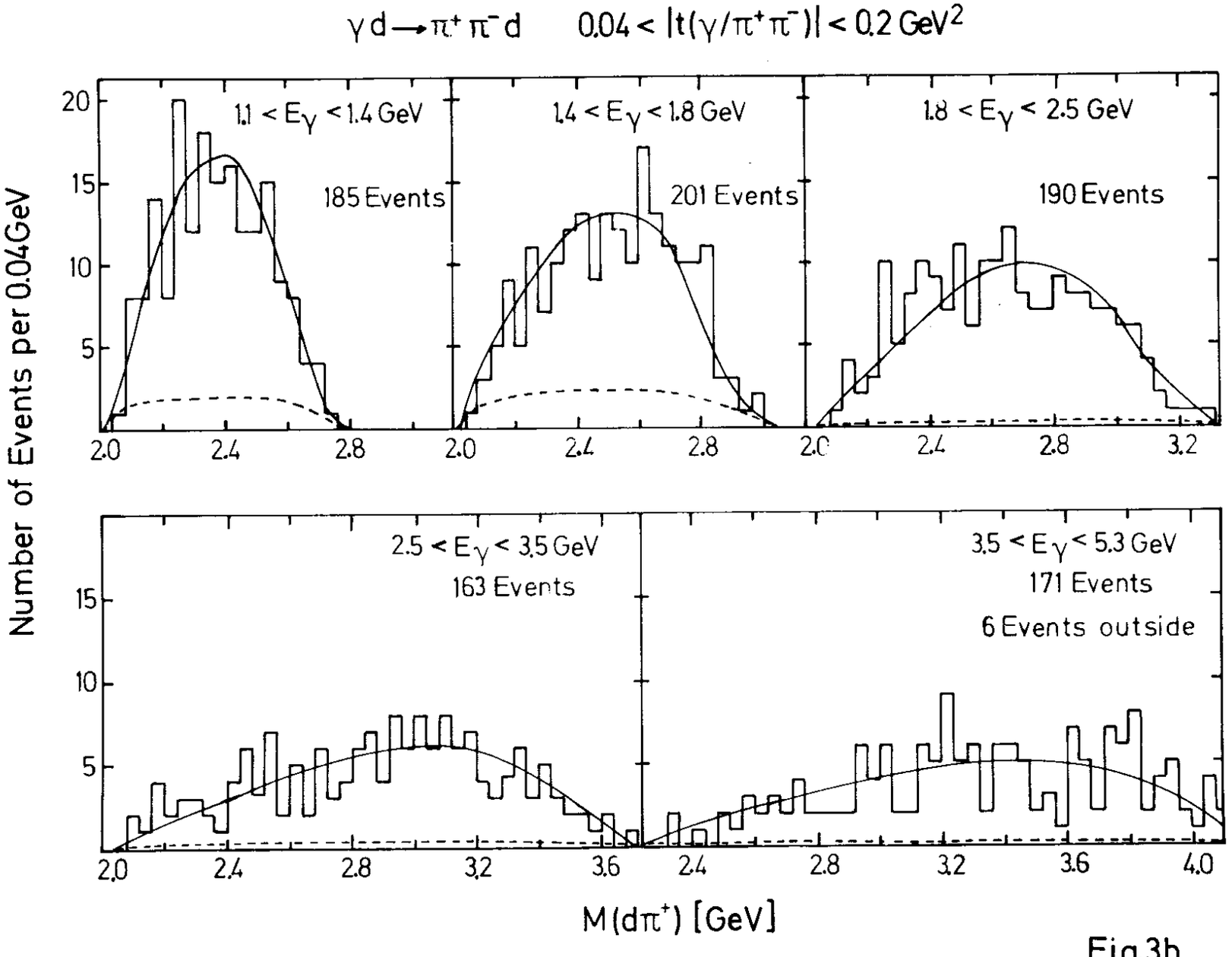
γ d → π⁺ π⁻ d 0.04 < |t(γ/π⁺π⁻)| < 0.2 GeV²
1.1 < Eγ < 1.4 GeV
185 Events
1.4 < Eγ < 1.8 GeV
201 Events
1.8 < Eγ < 2.5 GeV
190 Events
2.5 < Eγ < 3.5 GeV
163 Events
3.5 < Eγ < 5.3 GeV
171 Events
6 Events outside
Number of Events per 0.04GeV
M(dπ⁺) [GeV]

Fig.3b

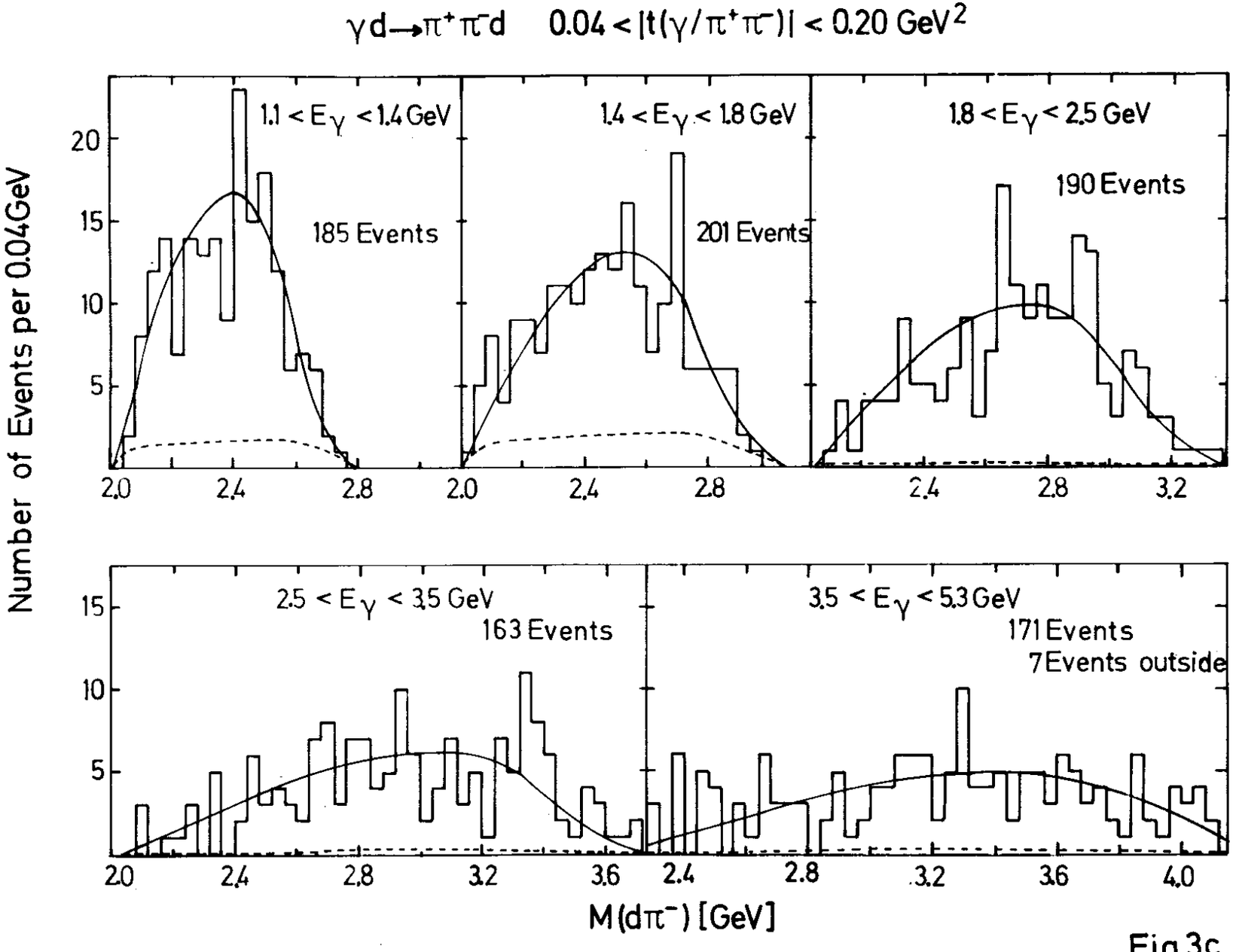
γd→π⁺π⁻d 0.04 < |t(γ/π⁺π⁻)| < 0.20 GeV²
1.1 < Eγ < 1.4 GeV
185 Events
1.4 < Eγ < 1.8 GeV
201 Events
1.8 < Eγ < 2.5 GeV
190 Events
2.5 < Eγ < 3.5 GeV
163 Events
3.5 < Eγ < 5.3 GeV
171 Events
7 Events outside
Number of Events per 0.04GeV
M(dπ⁻) [GeV]

Fig.3c

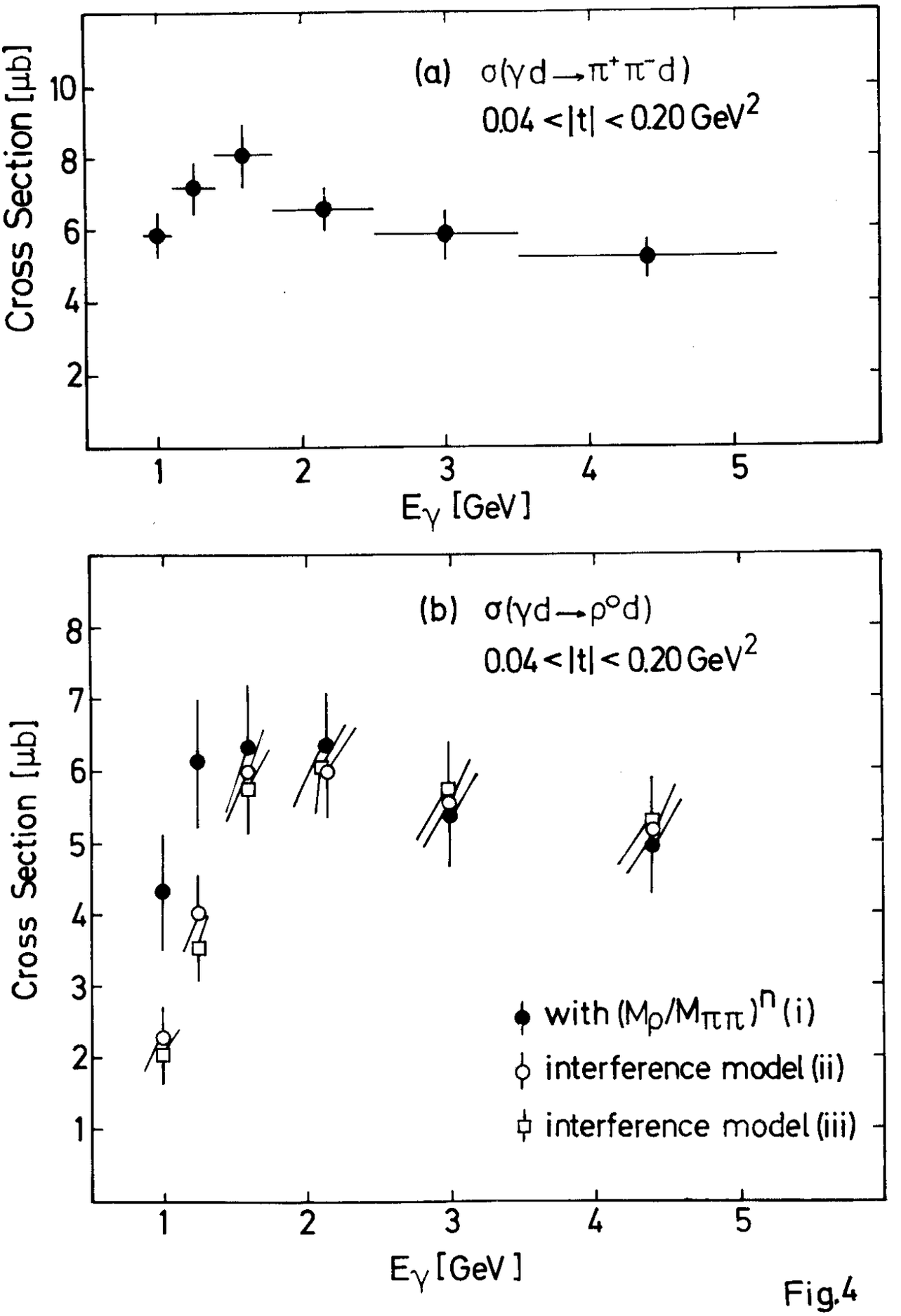
(a) σ(γd → π⁺π⁻d)
0.04 < |t| < 0.20 GeV²
Cross Section [μb]
Eγ [GeV]
(b) σ(γd → ρ°d)
0.04 < |t| < 0.20 GeV²
Cross Section [μb]
Eγ [GeV]
with (Mρ/Mππ)ⁿ (i)
interference model (ii)
interference model (iii)

Fig.4

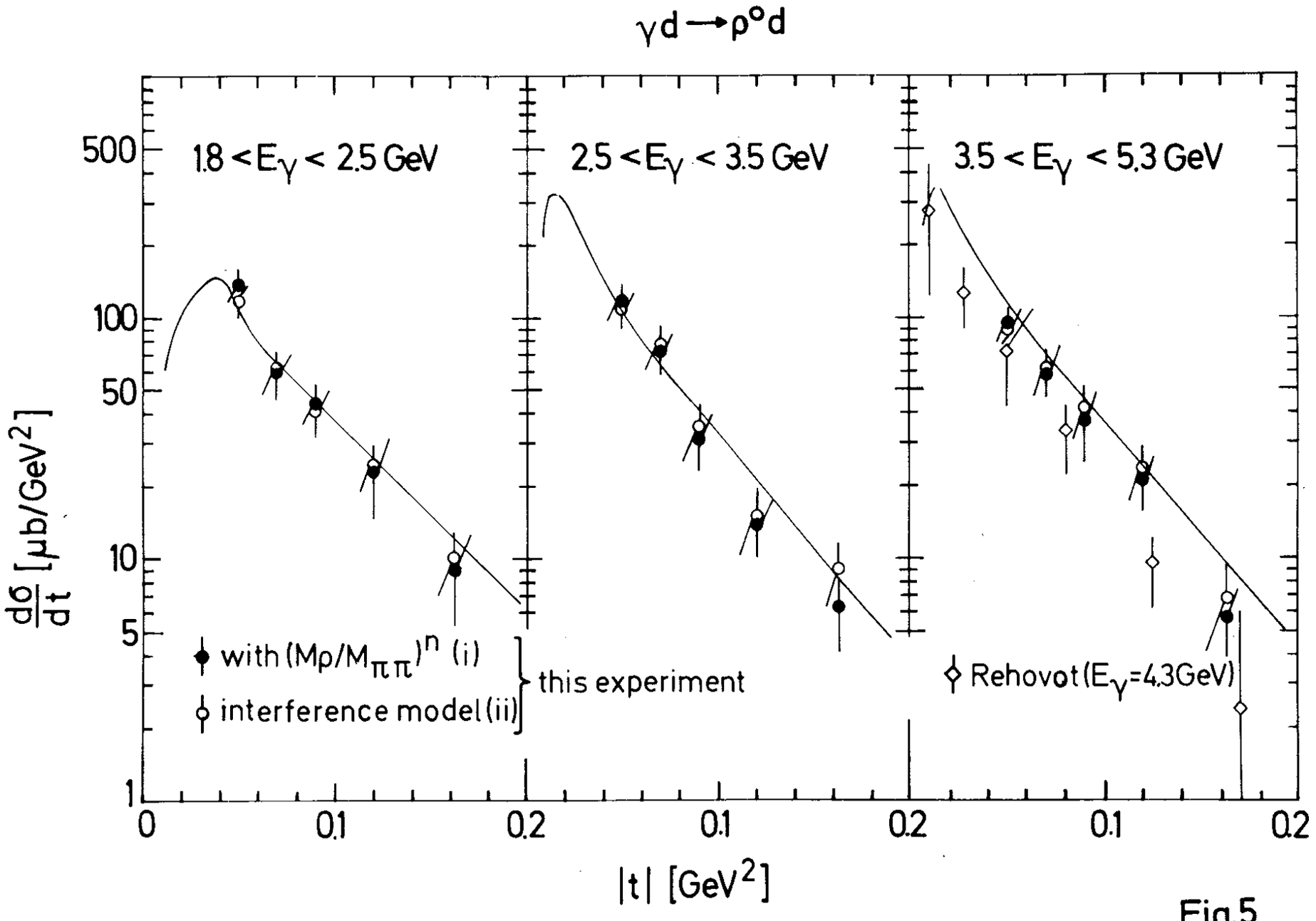
γd → ρ°d
1.8 < Eγ < 2.5 GeV
2.5 < Eγ < 3.5 GeV
3.5 < Eγ < 5.3 GeV
dσ/dt [μb/GeV²]
500
100
50
10
5
1
0
0.1
0.2
0.1
0.2
0.1
0.2
|t| [GeV²]
with (Mρ/Mππ)ⁿ (i)
interference model (ii)
this experiment
Rehovot (Eγ=4.3GeV)

Fig.5

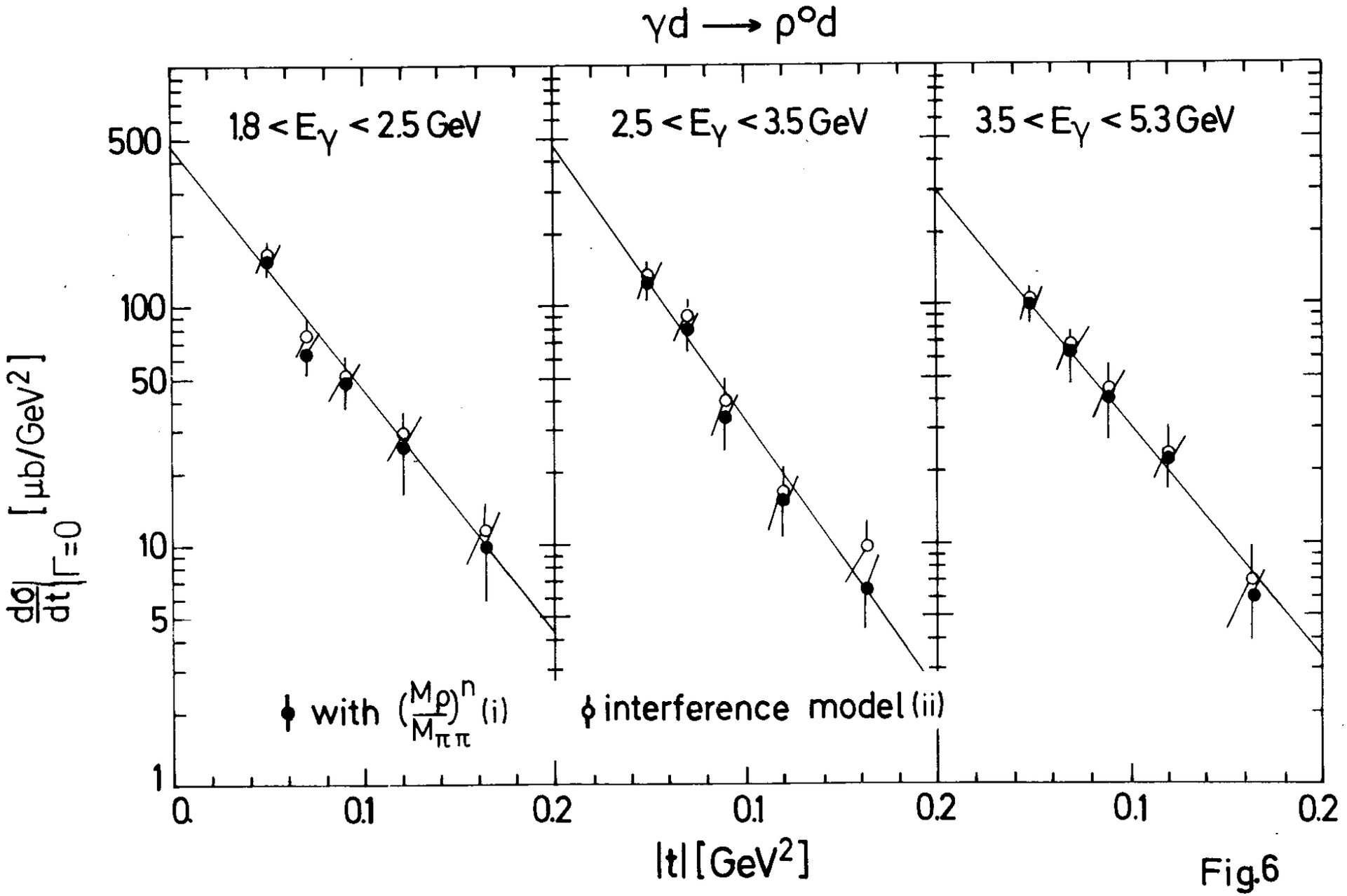
γd ⟶ ρ°d
1.8 < Eγ < 2.5 GeV
2.5 < Eγ < 3.5 GeV
3.5 < Eγ < 5.3 GeV
500
100
50
10
5
1
dσ/dt|Γ=0 [μb/GeV²]
with (Mρ/Mππ)^n (i)
interference model (ii)
0.
0.1
0.2
0.1
0.2
0.1
0.2
|t| [GeV²]

Fig.6

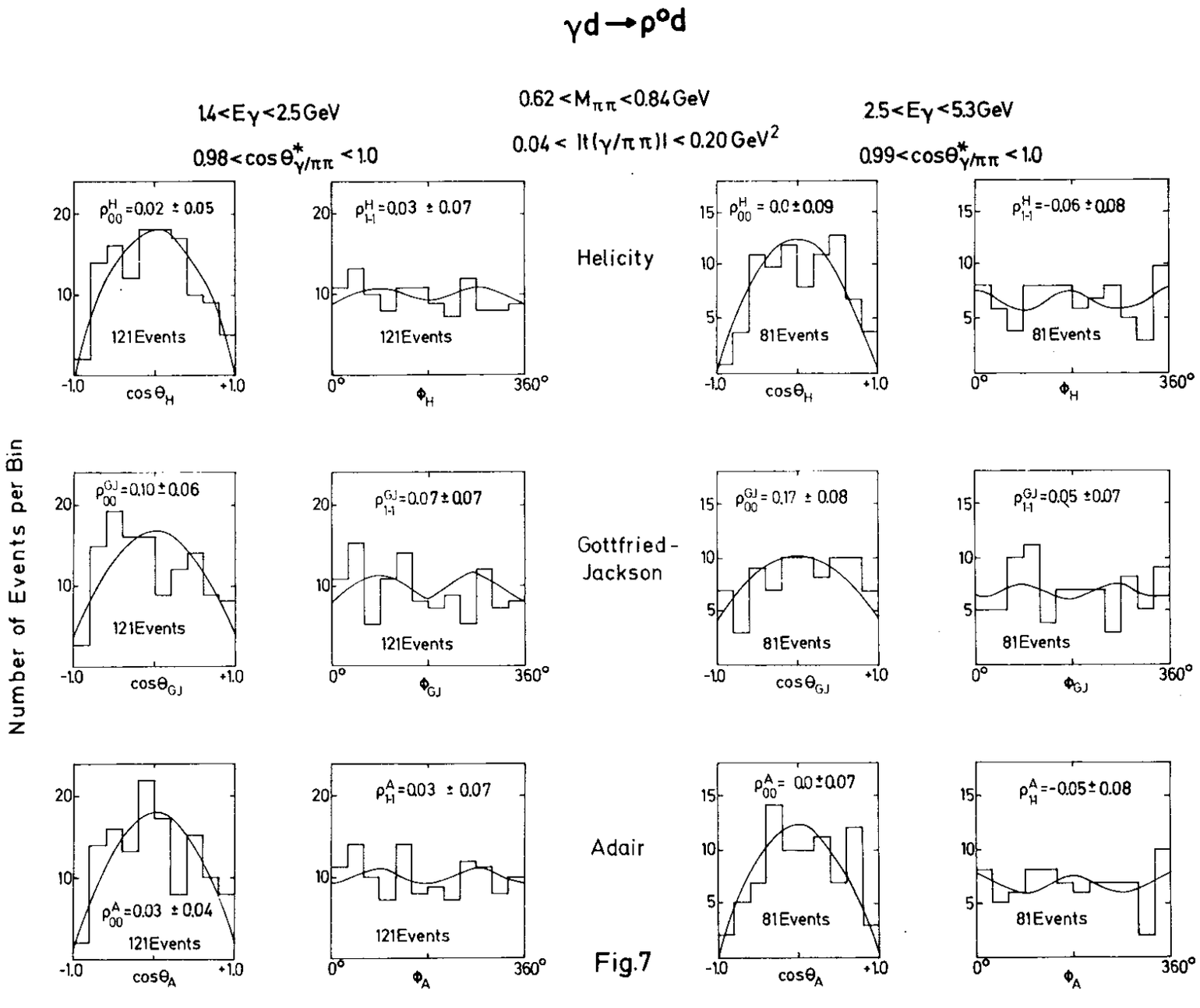
γd → ρ°d
1.4<Eγ<2.5GeV
0.98<cos θ*γ/ππ <1.0
0.62 <Mππ <0.84GeV
0.04 < |t(γ/ππ)| < 0.20 GeV²
2.5<Eγ<5.3GeV
0.99<cosθ*γ/ππ <1.0
Number of Events per Bin
Helicity
Gottfried - Jackson
Adair
ρ00H =0.02 ± 0.05
ρ1-1H =0.03 ± 0.07
ρ00H = 0.0 ± 0.09
ρ1-1H =-0.06 ± 0.08
ρ00GJ =0.10 ± 0.06
ρ1-1GJ =0.07 ± 0.07
ρ00GJ = 0.17 ± 0.08
ρ1-1GJ =0.05 ± 0.07
ρ00A =0.03 ± 0.04
ρ1-1A =0.03 ± 0.07
ρ00A = 0.0 ± 0.07
ρ1-1A =-0.05 ± 0.08
121Events
81Events
cosθH
ΦH
cosθGJ
ΦGJ
cosθA
ΦA
-1.0
+1.0
0°
360°

Fig.7

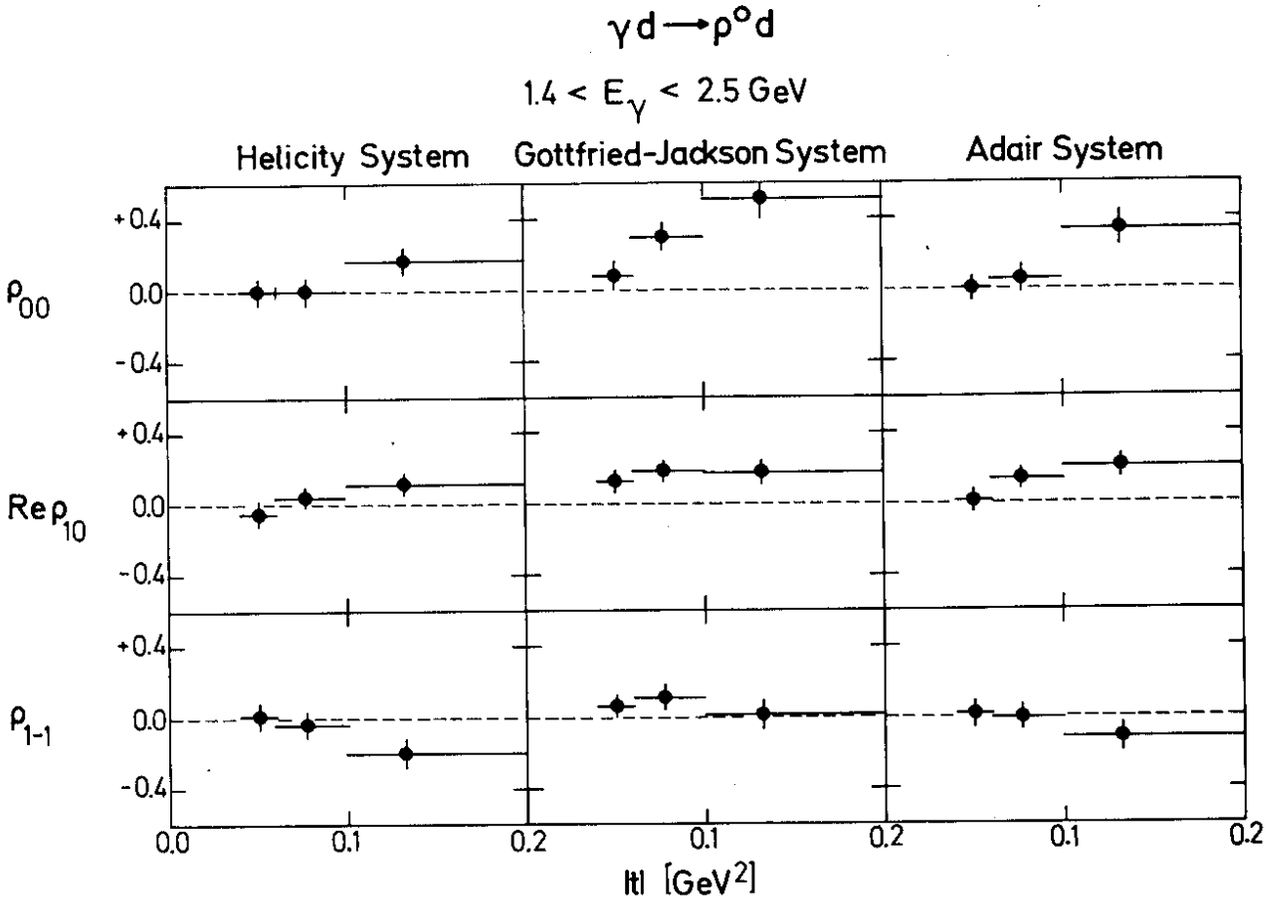
γd → ρ°d
1.4 < Eγ < 2.5 GeV
Helicity System
Gottfried-Jackson System
Adair System
ρ00
Re ρ10
ρ1-1
+0.4
0.0
-0.4
0.0
0.1
0.2
|t| [GeV2]

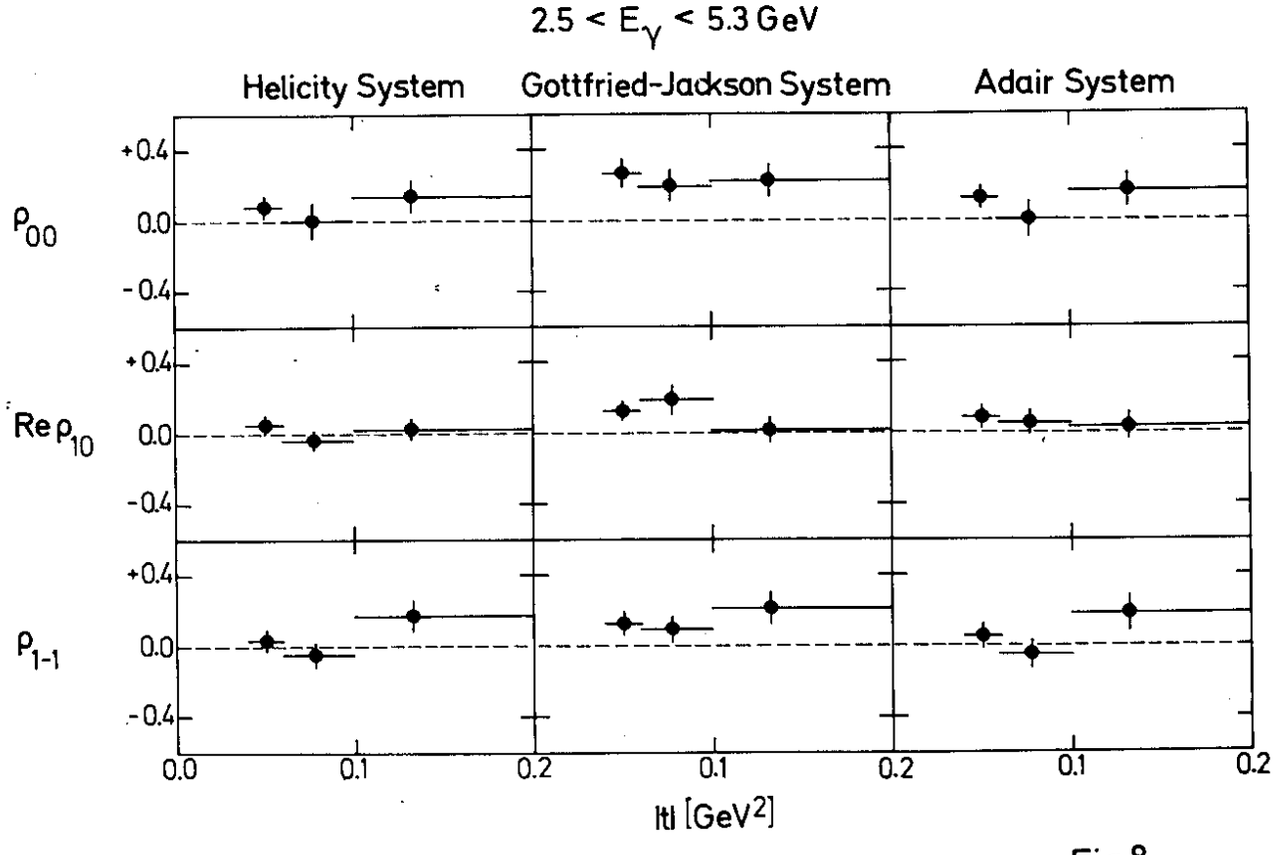
2.5 < Eγ < 5.3 GeV
Helicity System
Gottfried-Jackson System
Adair System
ρ00
Re ρ10
ρ1-1
+0.4
0.0
-0.4
0.0
0.1
0.2
|t| [GeV2]

Fig.8

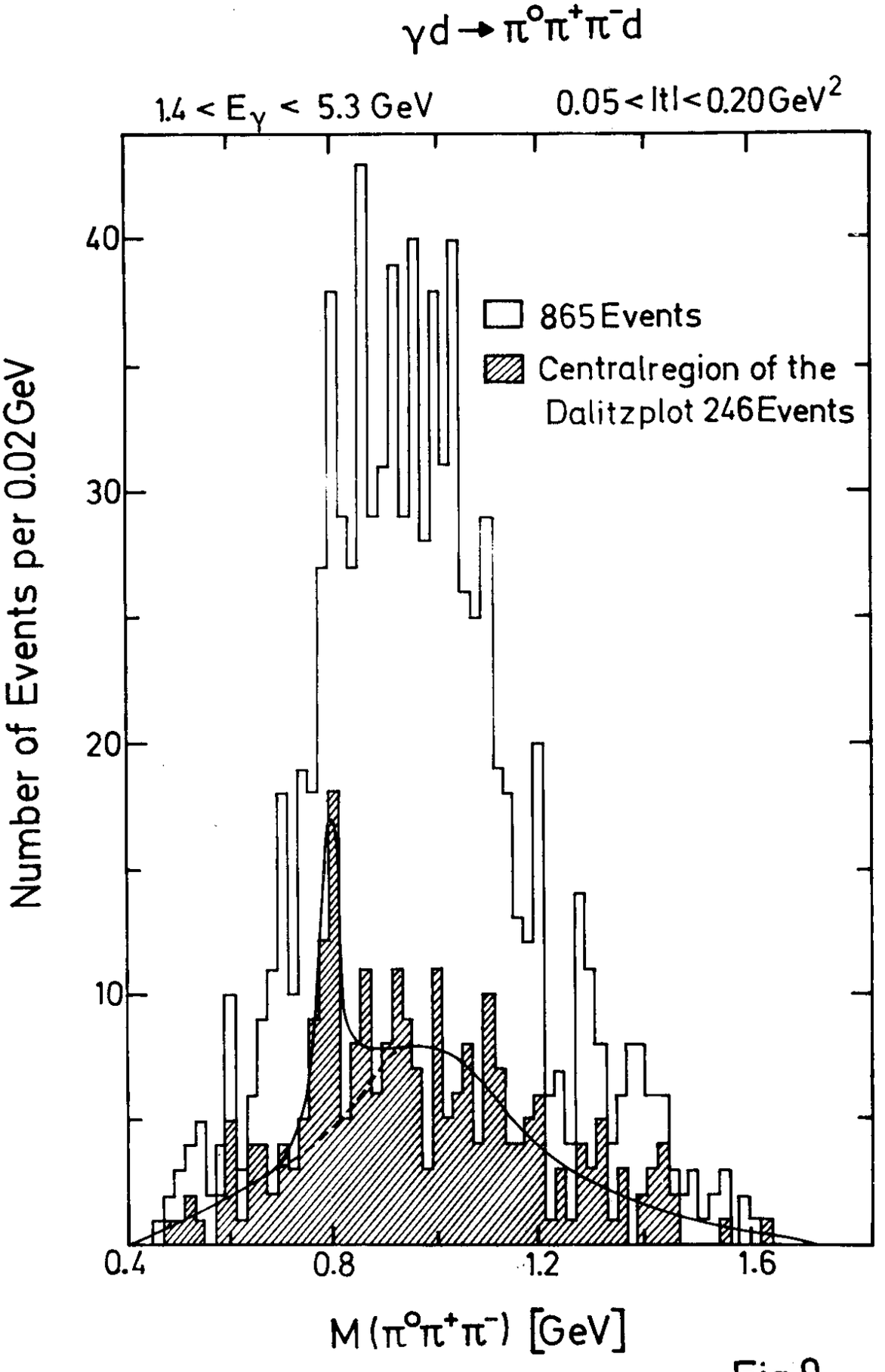
γd → π°π⁺π⁻d
1.4 < Eγ < 5.3 GeV
0.05 < |t| < 0.20 GeV²
865 Events
Centralregion of the Dalitzplot 246 Events
Number of Events per 0.02 GeV
40
30
20
10
0.4
0.8
1.2
1.6
M (π°π⁺π⁻) [GeV]

Fig.9

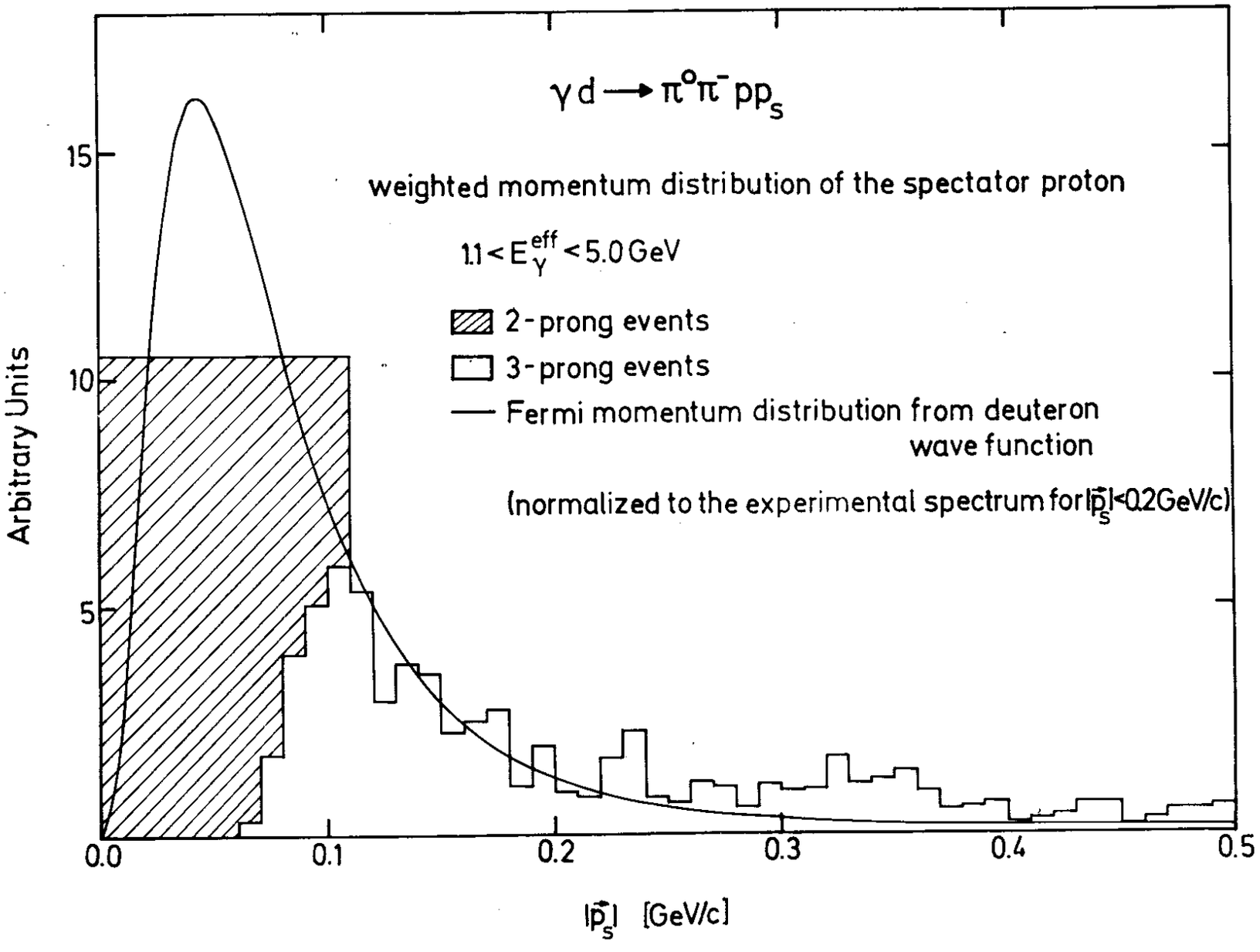
$\gamma d \longrightarrow \pi^0 \pi^- p p_s$
weighted momentum distribution of the spectator proton
$1.1 < E_\gamma^{eff} < 5.0$ GeV
2-prong events
3-prong events
Fermi momentum distribution from deuteron wave function
(normalized to the experimental spectrum for $|\vec{p}_s| < 0.2$ GeV/c)
Arbitrary Units
15
10
5
0.0
0.1
0.2
0.3
0.4
0.5
$|\vec{p}_s|$ [GeV/c]

Fig.10

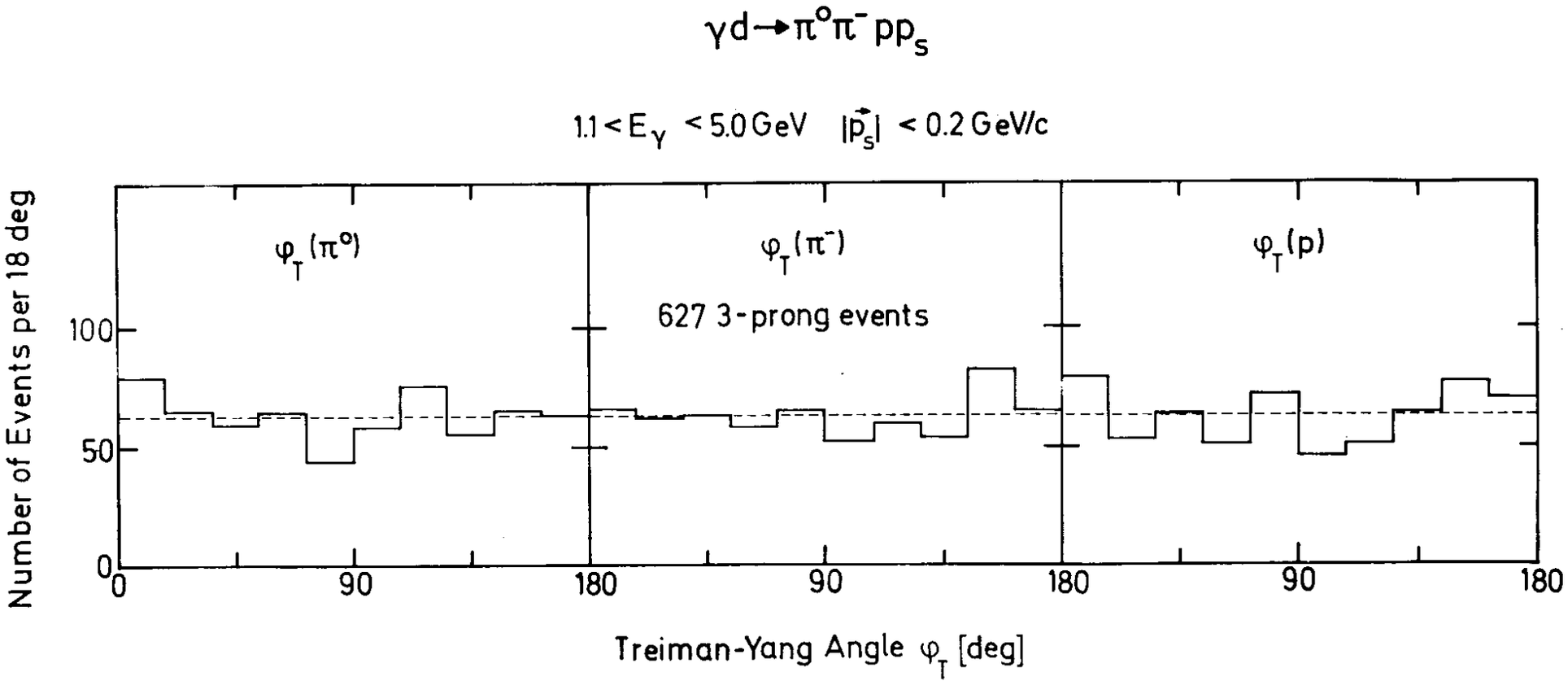
$\gamma d \rightarrow \pi^0 \pi^- p p_s$
$1.1 < E_\gamma < 5.0\,GeV \quad |\vec{p}_s| < 0.2\,GeV/c$
$\varphi_T(\pi^0)$
$\varphi_T(\pi^-)$
$\varphi_T(p)$
627 3-prong events
Number of Events per 18 deg
100
50
0
0
90
180
90
180
90
180
Treiman-Yang Angle φ_T [deg]

Fig.11

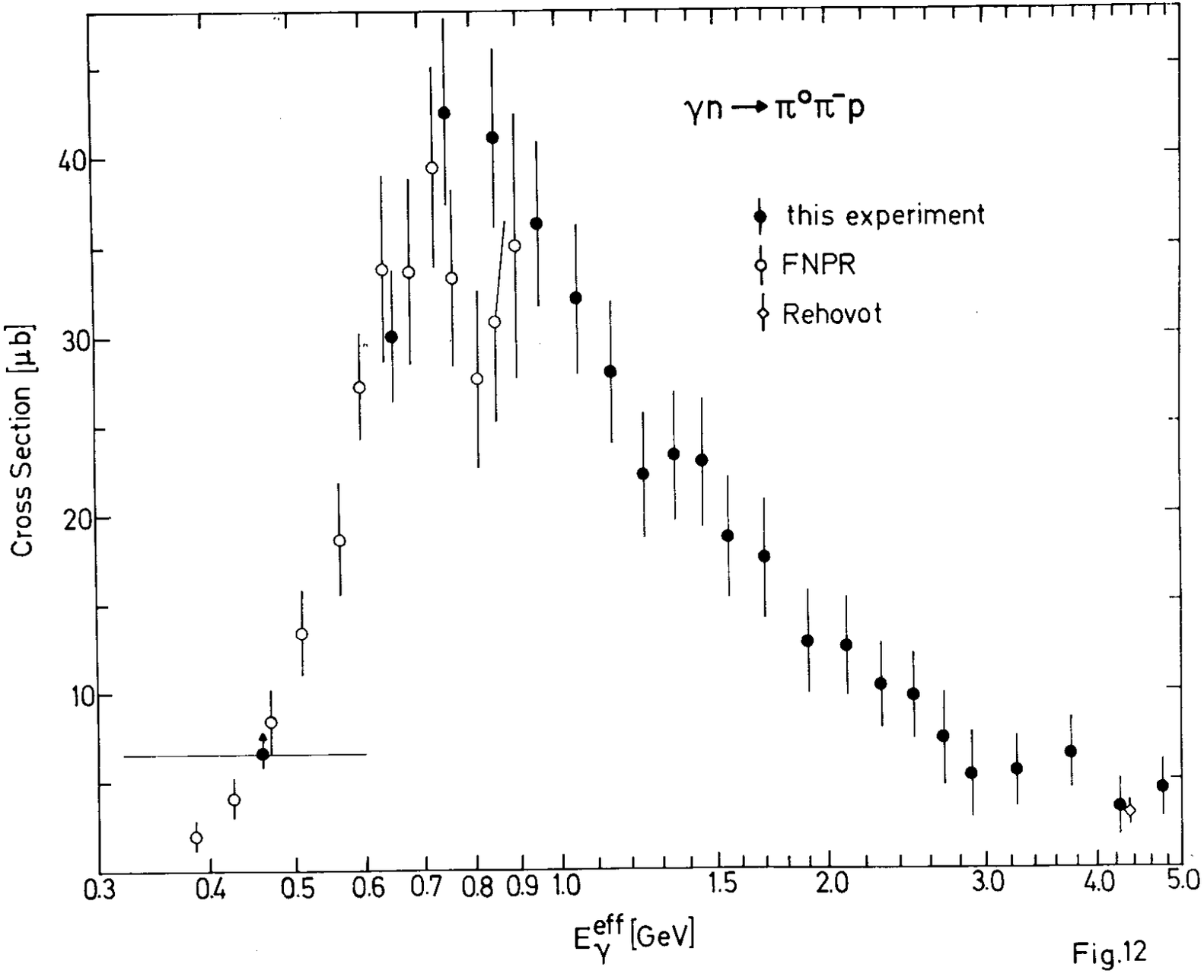
γn → π°π⁻p
this experiment
FNPR
Rehovot
Cross Section [μb]
40
30
20
10
0.3
0.4
0.5
0.6
0.7
0.8
0.9
1.0
1.5
2.0
3.0
4.0
5.0
E_γ^{eff} [GeV]

Fig.12

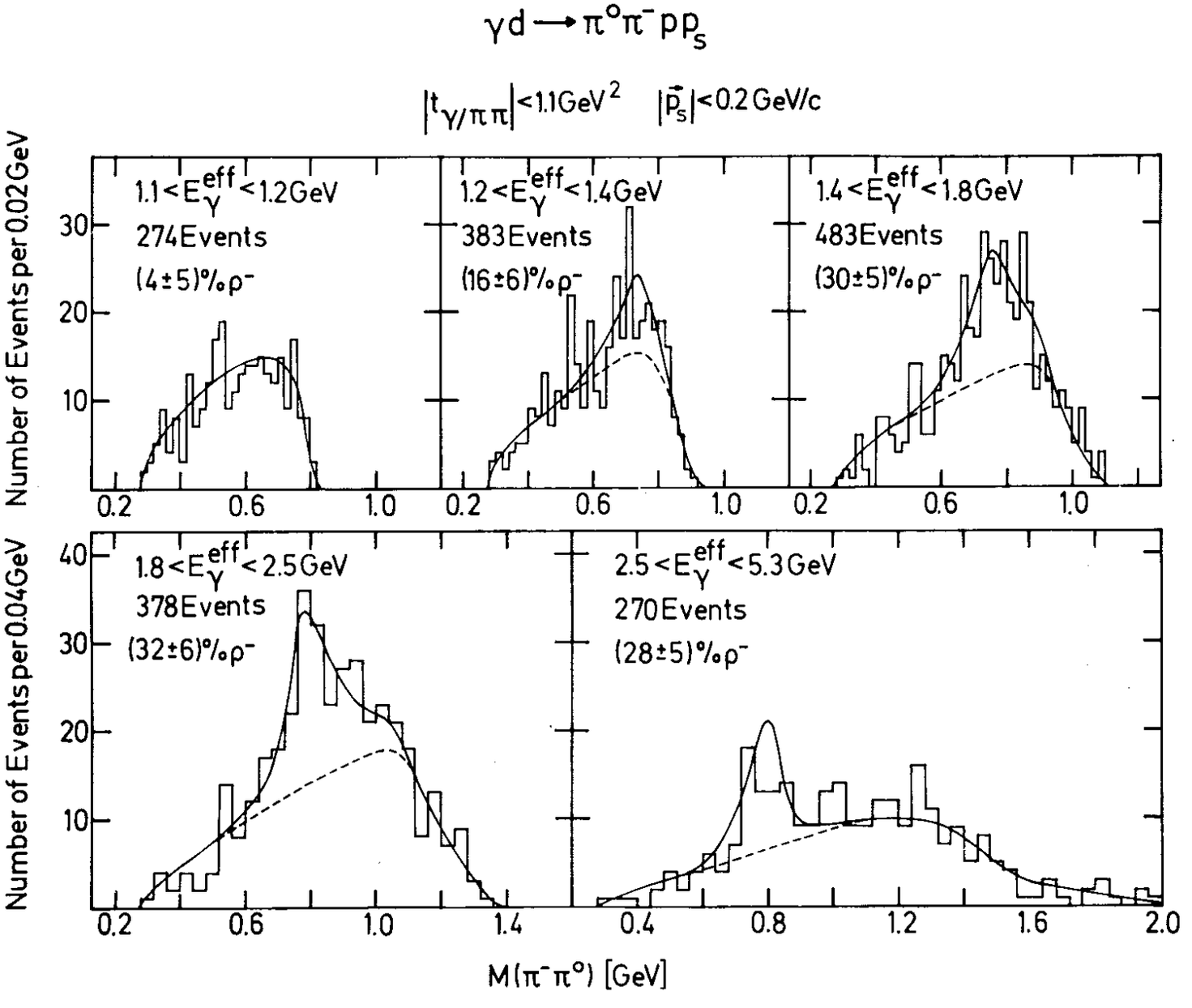
γd → π°π⁻pp_s
|t_γ/ππ| < 1.1 GeV² |p⃗_s| < 0.2 GeV/c
1.1 < E_γ^eff < 1.2 GeV
274 Events
(4±5)% ρ⁻
1.2 < E_γ^eff < 1.4 GeV
383 Events
(16±6)% ρ⁻
1.4 < E_γ^eff < 1.8 GeV
483 Events
(30±5)% ρ⁻
1.8 < E_γ^eff < 2.5 GeV
378 Events
(32±6)% ρ⁻
2.5 < E_γ^eff < 5.3 GeV
270 Events
(28±5)% ρ⁻
Number of Events per 0.02 GeV
Number of Events per 0.04 GeV
M(π⁻π°) [GeV]

Fig.13a

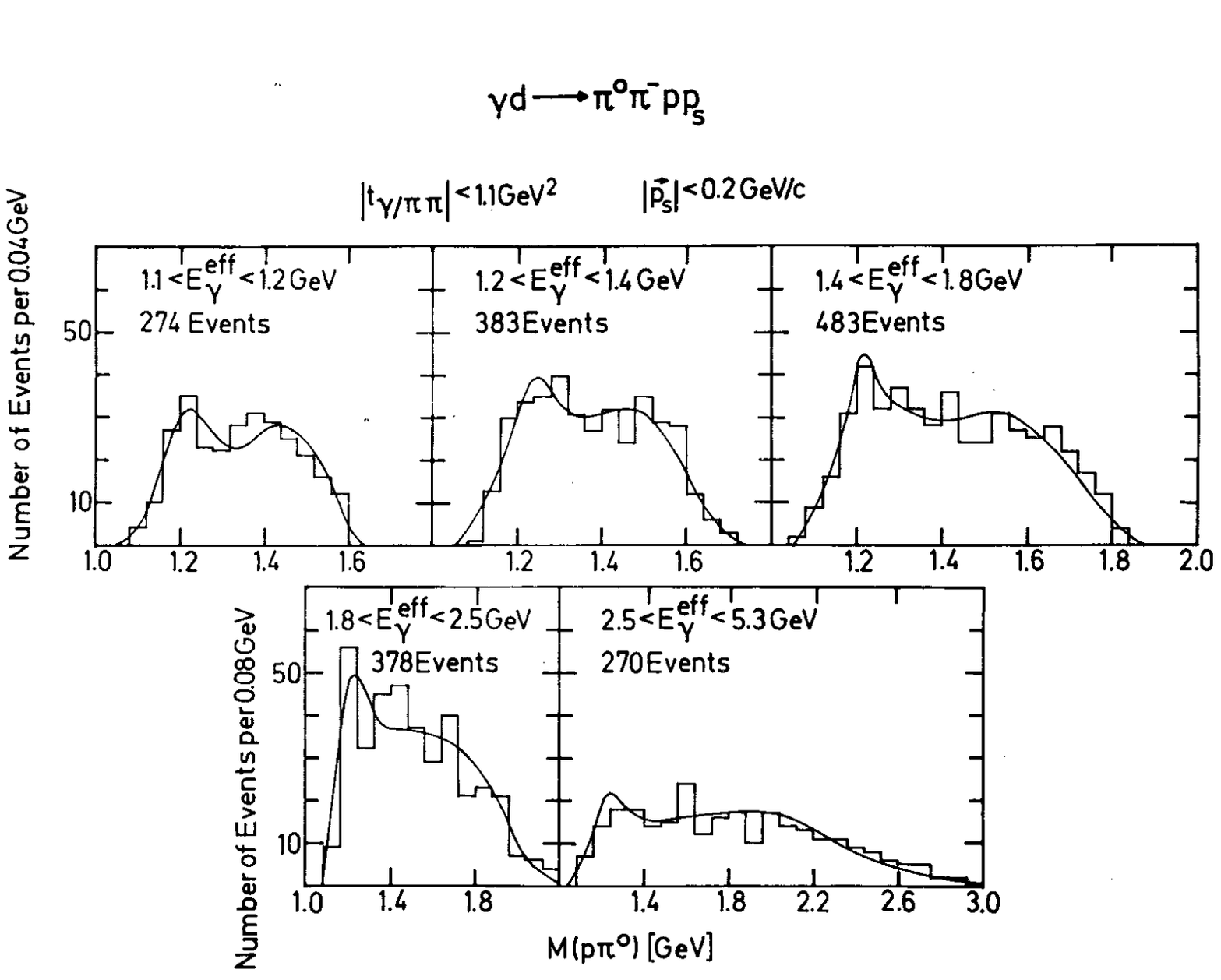
γd ⟶ π°π⁻pp_s
|t_γ/ππ| < 1.1 GeV²
|p⃗_s| < 0.2 GeV/c
1.1 < E_γ^eff < 1.2 GeV
274 Events
1.2 < E_γ^eff < 1.4 GeV
383 Events
1.4 < E_γ^eff < 1.8 GeV
483 Events
1.8 < E_γ^eff < 2.5 GeV
378 Events
2.5 < E_γ^eff < 5.3 GeV
270 Events
Number of Events per 0.04 GeV
Number of Events per 0.08 GeV
M(pπ°) [GeV]

Fig.13b

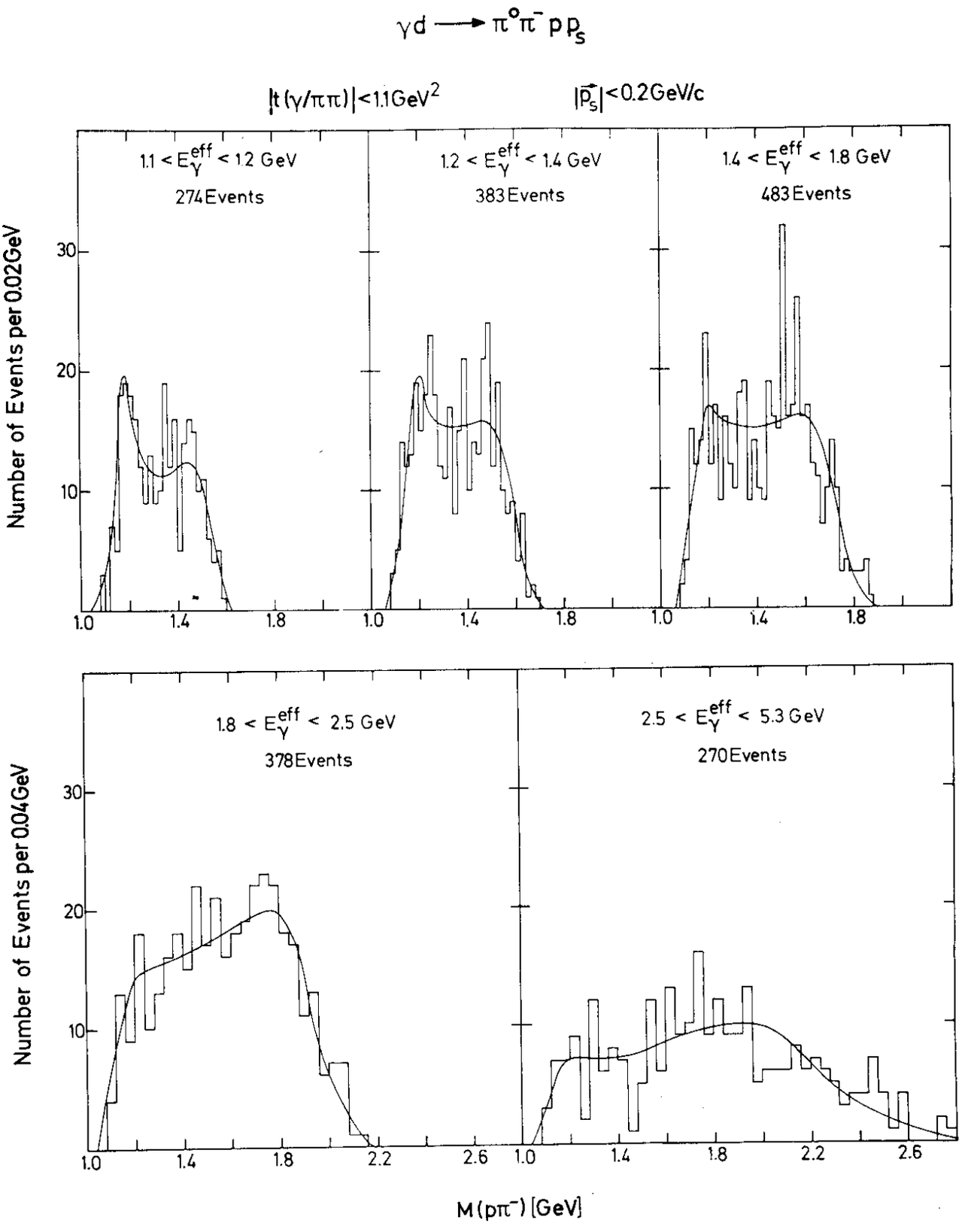
γd ⟶ π°π⁻ p p_s
|t(γ/ππ)|<1.1GeV²
|p⃗_s|<0.2GeV/c
1.1 < E_γ^eff < 1.2 GeV
274 Events
1.2 < E_γ^eff < 1.4 GeV
383 Events
1.4 < E_γ^eff < 1.8 GeV
483 Events
1.8 < E_γ^eff < 2.5 GeV
378 Events
2.5 < E_γ^eff < 5.3 GeV
270 Events
Number of Events per 0.02GeV
Number of Events per 0.04GeV
M(pπ⁻) [GeV]

Fig.13c

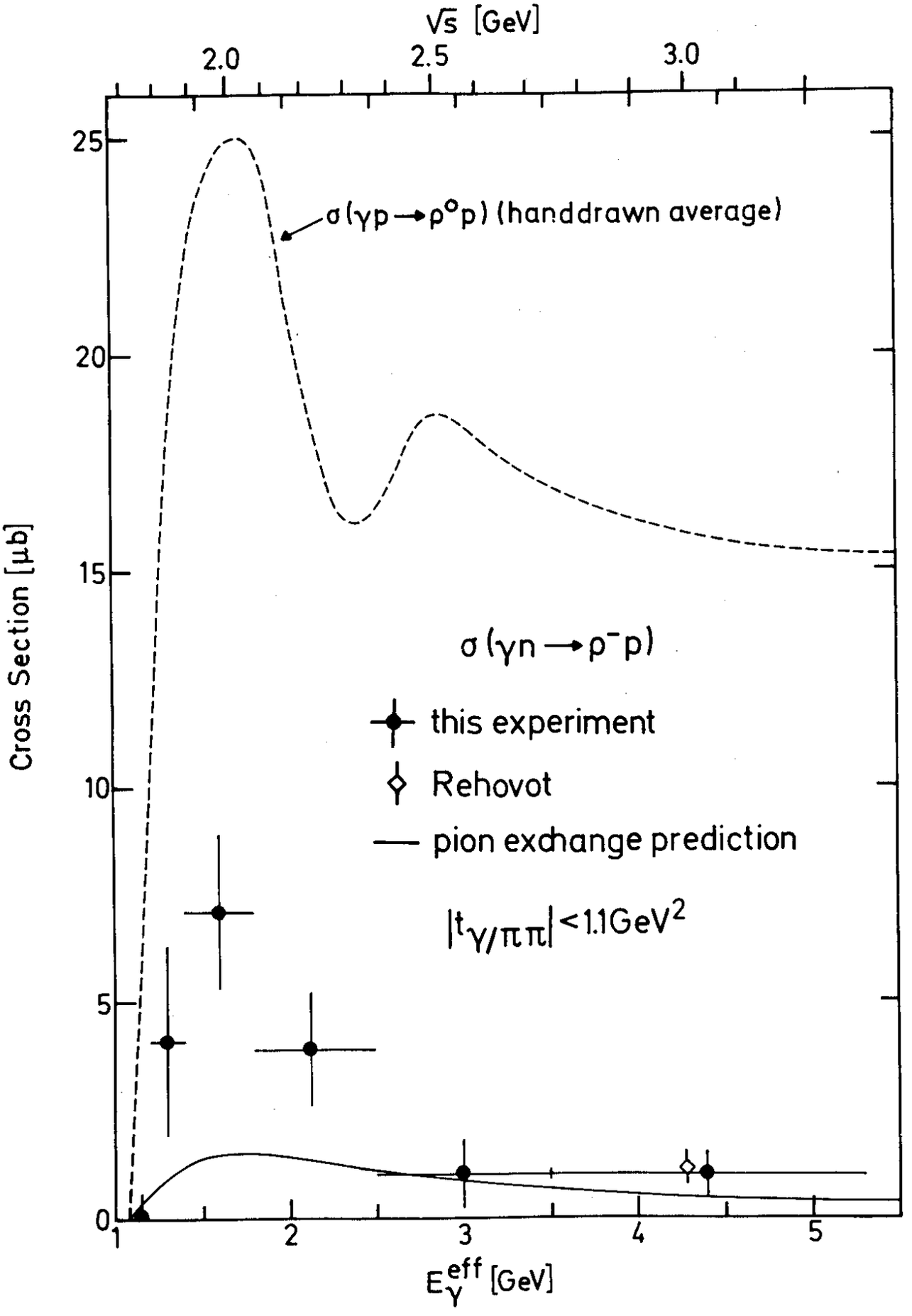
√s [GeV]
2.0
2.5
3.0
25
20
15
10
5
0
Cross Section [μb]
σ(γp → ρ°p) (handdrawn average)
σ(γn → ρ⁻p)
this experiment
Rehovot
pion exchange prediction
|t_γ/ππ| < 1.1GeV²
1
2
3
4
5
E_γ^eff [GeV]

Fig.14

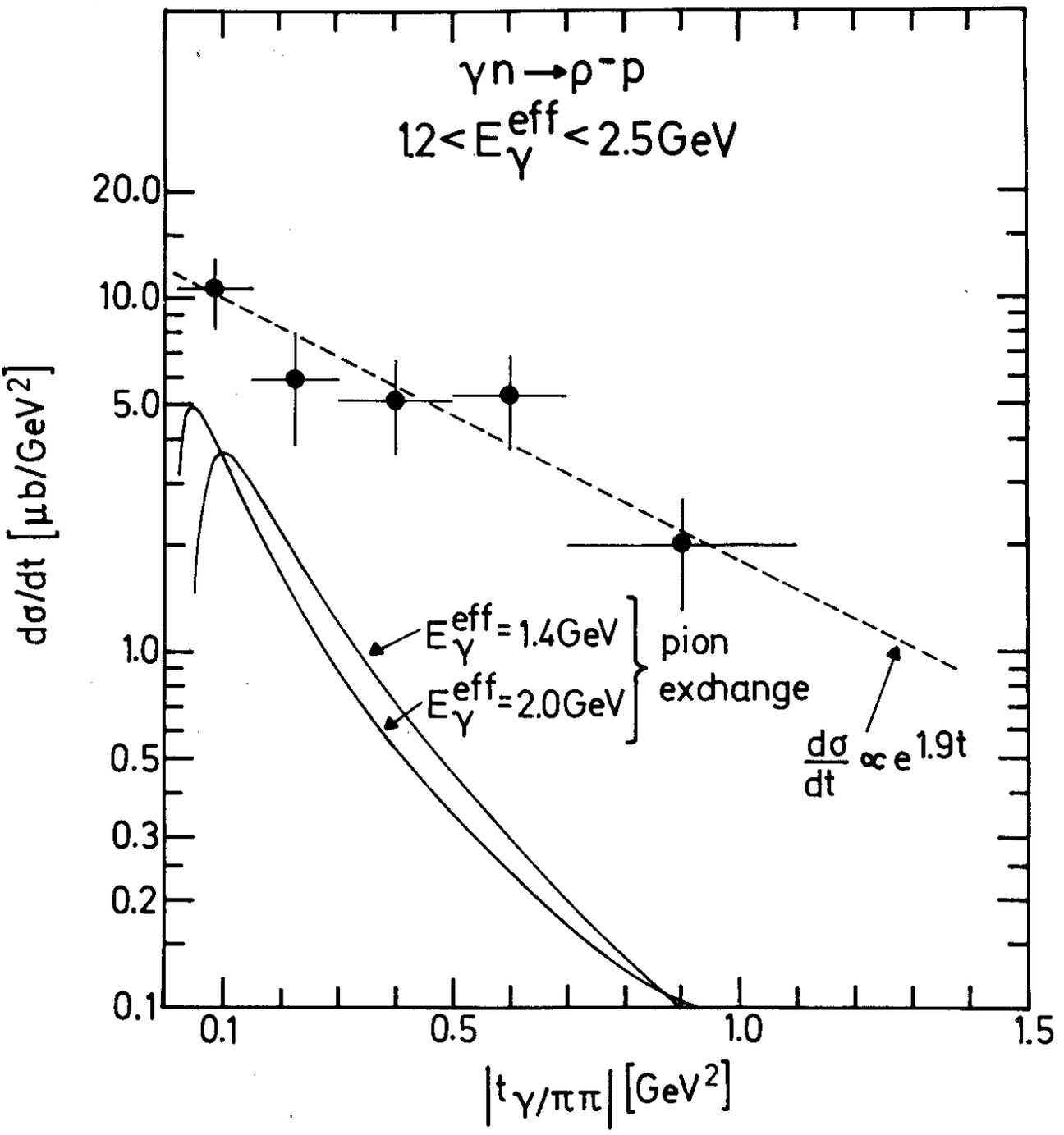
γn → ρ⁻p
1.2 < E_γ^eff < 2.5 GeV
dσ/dt [μb/GeV²]
20.0
10.0
5.0
1.0
0.5
0.3
0.2
0.1
0.1
0.5
1.0
1.5
|t_γ/ππ| [GeV²]
E_γ^eff = 1.4 GeV
E_γ^eff = 2.0 GeV
pion exchange
dσ/dt ∝ e^1.9t

Fig.15